

Temperature effects on water hammer phenomena in pipelines

Star, S. K.; Penuela Escobar, L. F.; van Meerkerk, M.; Pothof, I. W.M.; Heinsbroek, A. G.T.J.

DOI

[10.1016/j.applthermaleng.2024.125408](https://doi.org/10.1016/j.applthermaleng.2024.125408)

Publication date

2025

Document Version

Final published version

Published in

Applied Thermal Engineering

Citation (APA)

Star, S. K., Penuela Escobar, L. F., van Meerkerk, M., Pothof, I. W. M., & Heinsbroek, A. G. T. J. (2025). Temperature effects on water hammer phenomena in pipelines. *Applied Thermal Engineering*, 264, Article 125408. <https://doi.org/10.1016/j.applthermaleng.2024.125408>

Important note

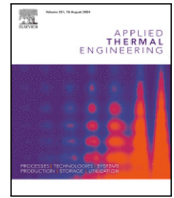
To cite this publication, please use the final published version (if applicable). Please check the document version above.

Copyright

Other than for strictly personal use, it is not permitted to download, forward or distribute the text or part of it, without the consent of the author(s) and/or copyright holder(s), unless the work is under an open content license such as Creative Commons.

Takedown policy

Please contact us and provide details if you believe this document breaches copyrights. We will remove access to the work immediately and investigate your claim.



Research Paper

Temperature effects on water hammer phenomena in pipelines

S.K. Star ^a, L.F. Penuela Escobar ^a, M. van Meerkerk ^a, I.W.M. Pothof ^{a,b},
A.G.T.J. Heinsbroek ^a

^a Department of Hydraulics for Industry and Infrastructure, Deltares, Delft, The Netherlands

^b Department of Water Management, Sustainable Heating & Cooling, TU Delft, Delft, The Netherlands

ARTICLE INFO

Keywords:

Water hammer phenomenon
District heating systems
Thermal-hydraulic modeling
Cavitation effects
Pipeline material properties
Transient pressure surges

ABSTRACT

Water hammer, or hydraulic shock, occurs in pressurized pipelines when fluid flow is abruptly altered, leading to pressure surges. Even though this phenomenon can cause significant damage to systems, it is often overlooked during design phases of district heating (DH) networks. This paper investigates the impact of temperature on water hammer phenomena. Various modeling approaches are discussed, emphasizing the importance of considering both hydraulic and thermal transients. To assess the impact, we modeled and simulated a reference problem involving rapid valve closure in a copper pipe system, considering both cavitating and non-cavitating flow scenarios. The steady-state results show that the pressure head at the downstream end of the pipe increases with temperature due to decreasing density and is independent of the pipe material properties. The transient results reveal that higher temperatures lead to cavitation and more intense pressure peaks, which could be missed without considering thermal-hydraulic phenomena. The analysis of a practical problem involving a 1000 MW DH system in Helsinki showed that using a single wave speed for both supply and return lines underestimates pressure peaks due to partial wave cancellation. In contrast, temperature-dependent wave speeds provide more accurate predictions of pressure wave behavior, highlighting the importance of understanding these effects. Sudden pressure drops can trigger protective measures and lead to cavitation, weakening pipeline integrity over time. The findings underscore the importance of considering temperature-dependent properties in the design, modeling and analysis of DH networks to prevent potential damage and ensure system reliability.

1. Introduction

Water hammer, also known as hydraulic shock, occurs in pressurized pipelines when a fluid, such as water, experiences sudden deceleration or acceleration. This phenomenon can occur in both single-phase and multiphase flows and can be triggered by events such as pump failure, pump start, rapid valve closure, or the filling of normally empty systems. In these instances, changes in fluid velocity are directly linked to pressure changes, which propagate rapidly as waves (pressure surges or water hammer) through the pipeline system. Additional mechanisms can also induce water hammer events, such as rapid condensation of steam in two-phase flow environments, leading to local but violent impacts of water slugs [1], or the presence of entrapped air or gas pockets [2]. Fluid–structure interaction due to pipeline motion, for example during earthquakes, is another contributing factor [3].

In severe cases, water hammer can cause significant damage, including pipe ruptures or complete displacement of the pipe at specific points. More commonly, the process occurs gradually, with each water hammer event progressively weakening the pipe until rupture occurs.

Water hammer is often identifiable by a loud banging or knocking sound, particularly if the pipe is not well anchored [4,5].

In the fields of drinking water and wastewater management, water hammer analysis is routinely conducted during system renewal, expansion, or replacement, as well as in the detailed design phase [6]. This analysis helps identify operational risks and mitigation measures for both current and future scenarios. However, in the field of district heating (DH) systems, recent advisory projects by Deltares, an independent institute for applied research in the field of water, subsurface and infrastructure, along with handbooks and literature [7,8], indicate that water hammer analysis often receives insufficient attention. This analysis is not yet standard practice during system design phases. Additionally, analyzing water hammer in district heating pipelines through full-scale experiments is prohibitively costly due to the large scale. Furthermore, replicating the physical properties of pipes in scale models is challenging and adds to the difficulty [9]. This oversight can hinder the development of district heating networks, which are important for

* Corresponding author.

E-mail address: Kelbij.Star@Deltares.nl (S.K. Star).

Nomenclature**Latin Letters**

\dot{m}	Mass flow rate (kg/s)
A	Cross-sectional flow area (m ²)
a	Material-specific constant (–)
c	Wave speed (m/s)
c_p	Specific heat (J/kg K)
D	Inner diameter of the pipe (m)
Δs	Element length (m)
dt	Time step (s)
E	Young's modulus (Pa)
e	Wall thickness of the pipe (m)
f	Darcy–Weisbach friction factor (–)
g	Gravitational acceleration (m/s ²)
H	Head (m)
H_v	Vapor head (m)
i	Observed element (–)
K	Bulk modulus (Pa)
k	Thermal conductivity (W/m K)
k	Wall roughness (m)
L	Length of the pipe (m)
m	Exponent for valve closure curve (–)
N	Number of pipe elements (–)
n	Number of time steps (–)
p	Pressure (Pa)
p_v	Vapor pressure (Pa)
p_{atm}	Atmospheric pressure (Pa)
Q	Discharge (m ³ /s)
Q_{loss}	Heat loss (W)
q_{loss}	Heat loss per unit volume (W/m ³)
T	Temperature (°C)
t	Time (s)
t_c	Characteristic time constant (s)
u	Internal energy (J/kg)
V	Volume (m ³)
v	Velocity (m/s)
V_0	Initial volume (m ³)
z	Height relative to the horizontal reference plane (m)
Re	Reynolds number (–)

Greek Letters

β	Fraction of friction converted to heat loss (–)
Δs	Element length (m)
Δt	Time step (s)
ν	Kinematic viscosity (m ² /s)
ψ	Axial pipe constraint parameter (–)
ρ_f	Fluid density (kg/m ³)
τ_v	Valve closure factor (–)

Abbreviations

1D	One-dimensional
BC	Boundary condition
DGCM	Discrete Gas Cavity Model

DH	District heating
DVCM	Discrete Vapor Cavity Model
HDPE	High-density polyethylene
HT	High temperature
HX	Heat exchanger
MoC	Method of Characteristics
MT	Medium temperature
NPP	Nuclear Power Plant
PE	Polyethylene
PUR	Polyurethane

Subscripts

0	Reference, initial or upstream side of the pipe
L	Downstream side of the pipe

Table 1

Examples of operational and projected district heating networks supply and return line temperatures in Europe.

Location	Supply (°C)	Return (°C)	Heat source	Status 2021	Ref.
Aalborg (Denmark)	60–65	40	Residual heat (cement factory)	Operational	[19]
Salaspils (Latvia)	90–60	60–35	Solar	Operational	[19]
Madrid-Mostoles (Spain)	90	70	Biomass	Operational	[19]
Amsterdam (The Netherlands)	120	85	Waste heat (data center)	Projected	[20]
Berlin (Germany)	70	40	Waste heat (data center)	Projected	[21]
Madrid (Spain)	50–55	25–35	Hospital (cooling)	Projected	[22]

the energy transition [10–12]. District heating and cooling systems are projected to see significant growth, with energy supplied to be expected to double in the EU-27 countries [13] and increase from 30 PJ in 2024 to approximately 40 PJ in 2030 in the Netherlands [14,15]. Additionally, the financial costs and energy associated with repairing and optimizing poorly designed systems can be significant [16]. Therefore, emphasizing water hammer risks to designers and operators is crucial for the successful operation and scaling of district heating systems.

Thus, in the Dutch district heating sector, water hammer appears to be insufficiently recognized during system design. This raises the question of whether this oversight is justified. District heating networks consist of pressurized pipes similar to those used in drinking water and wastewater systems, where events that cause water hammer, such as pump trips and sudden valve closures, can occur. However, there are differences, as district heating networks often form closed loops, operate at higher temperatures, and have different temperatures between supply and return pipes. Fig. 1 shows the typical supply and return temperatures across various types of district heating networks, with medium temperature (MT) networks having a supply temperature up to 90 °C. Current supply and return temperatures in Denmark, which has a climate comparable to the Netherlands [17], are as low as 70/40 °C on average [18]. However, significant energy savings can be achieved by reducing the supply and return temperatures, e.g. from 80/40 to 60/30 °C. Table 1 summarizes some examples of operational and planned district heating networks with their supply and return temperatures.

Another thing to note is that during the initial operation of heating networks, water hammer may not be noticeable because the network operates below its maximum capacity. However, as more households

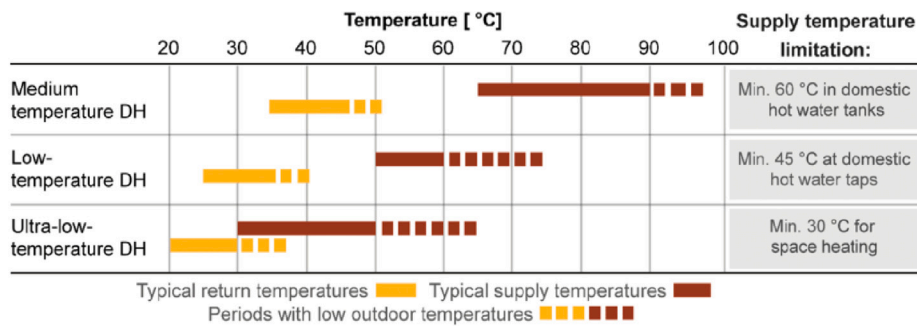


Fig. 1. Typical supply and return temperatures in different types of district heating networks [18]. Network temperature levels.

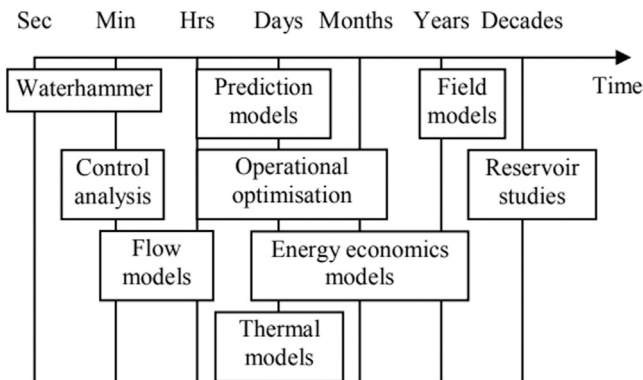


Fig. 2. Different time scales for simulations of district heating systems can be used [23].

connect and the network approaches full capacity, the risk of problems will increase if water hammer has not been addressed during the design phase. The hydraulic load may also increase if the mass flow is increased to compensate for a reduced design temperature difference at reduced network temperatures; e.g. transforming a network from 100/60 to 80/50 °C at the same design power, will lead to 33% increase in design mass flow rate.

For these reasons, addressing water hammer during the design phase is essential to prevent future issues when district heating networks experience heavier loads. To effectively manage these challenges, it is crucial to employ accurate simulation models. District heating systems can be modeled and simulated in many different ways. Wernstedt et al. [23] indicated that the purpose of simulation models of district heating systems is to capture the time dependent behavior of the system. They showed that many different time scales can be used for the simulations. Fig. 2 gives a clear overview of this. Fast transient behavior, such as water hammer, occurs in the order of seconds to minutes, while strategical studies require simulating years, decades or even longer.

Based on literature, common (numerical) models can be classified into three main categories according to how time dependency is considered: steady-state, dynamic with simplified modeling of physics and dynamic with a detailed modeling of physics [24]. However, for the dynamic modeling of thermal-hydraulic networks, including district heating networks, we distinguish here between the following three categories: (i) Pseudo-dynamic models that treat hydraulics as a steady-state phenomenon while dynamically solving thermal transients, (ii) dynamic hydraulic models that treat hydraulics dynamically but neglect or assume steady thermal phenomena, and finally (iii) fully dynamic thermal-hydraulic models that treat both the hydraulics and thermal phenomena dynamically. Table 2 summarizes this classification.

The most common (numerical) model for thermal-hydraulic networks, including district heating networks, is pseudo-dynamic. This

Table 2

Different dynamic model types and physical phenomena.

Model type	Hydraulic phenomena	Thermal phenomena
Pseudo-dynamic	(Quasi)-steady-state	Transient
Dynamic hydraulic	Transient	Steady-state or neglecting
Fully dynamic	Transient	Transient

model treats hydraulics as a (quasi)-steady-state phenomenon while dynamically solving thermal transients [25–28]. It is often preferred due to the rapid advancement of pressure waves compared to the low convective velocity of DH water [29], with pressure changes propagating approximately 1000 times faster than temperature changes [25]. Giraud et al. [30] and Guelpa [31] support this approach. They note that pressure waves propagate through a hydraulic network at a velocity exceeding 1000 m/s. The travel time of those waves rarely exceeds one minute in a DH system. This is smaller than the time steps usually adopted for calculations (mainly larger than 60 s) [31]. Also, the settling time to reach a new steady-state will be shorter than the time to reach a new thermal equilibrium of a system. Therefore, they motivated that the dynamic term that accounts for the rate of change in the momentum balance for each component model can be neglected. Similarly, Oppelt et al. [32] described the network model as comprising a quasi-static hydraulic model and a transient thermal model, based on tracking water segments through the whole network.

On the other hand, there are models that only exploit the dynamic treatment of hydraulics in thermal-hydraulic networks. Paananen and Henttonen [33] focused on several transients including pump trips and leaks in a 77 km long-distance heat transport system to transport 1000 MW of heat. Their study used a computer model and simulation to examine the behavior of such a large-scale heat transport system. In addition, safety analyses were conducted to support preliminary planning of the system. However, the study did not account for wave speed changes between supply and return line. Similarly, Kaliatka et al. [34] presented three hypothetical accident scenarios in the Kaunas city heating network, including a blackout in the central pump station, a break of the heat supply pipe to the northwestern district, and a rapid pump trip in one of the city's pump stations. The paper discussed dynamic processes, such as the water hammer effect, in pipelines during accidents. However, they only modeled the hydraulic phenomena, not the heat losses in the pipelines and heat removal in the consumers' heating systems. Also Zheng et al. [35] only performed hydraulic transient calculations for water hammer protection and rapid leakage detection in large-scale district heating networks based on hydraulic transient analysis. However, this model does not separately model supply and return lines.

Finally, there are models that consider both hydraulic and thermal transient phenomena. These are fully dynamic models that simulate both the temperature and the flow dynamically [27,29]. Examples include the work by Kallio [25] who emphasized that the KEU simulation model will be fully dynamic due the capabilities of the Apros simulation

software. Also, Stevanovic et al. [36] developed computer codes to simulate both hydraulics and thermal phenomena dynamically in DH systems. These codes are based on the high-order accurate numerical solution of the transient energy equation and the hydraulic prediction of pressure and fluid flow rates within the complex pipe network. Yet, from an operational optimization point of view, they noted that the dynamics of the flow in the network are of minor importance compared with the dynamics of the temperature changes. However, dynamics of flow and pressure waves is most important from a design perspective [6].

This highlights that different models serve for different purposes as Fig. 2 shows. Yet, it is not clear to what extent thermal phenomena need to be considered for water hammer studies in the design phase and whether a dynamic hydraulic model without considering temperature is sufficient or fully dynamic models are needed.

In this paper, we investigate the effect of temperature on water hammer phenomena. We focus here on water hammer events that are caused by deceleration of single-phase liquids flowing in a piping system for heating. Section 2 explores the effect of temperature on the wave speed considering fluid and material properties. Section 3 explains some details about the Wanda software used in this study. A reference and a practical problem are presented in Sections 4 and 5, respectively. Finally, Section 6 offers conclusions and recommendations.

2. Temperature effect on water hammer phenomena in pipeline systems

There are a few studies in literature that discussed the effect of temperature on water hammer phenomena. We highlight a couple of them here. Emadi and Solemani [37] investigated the effect of various input parameters. These include water temperature, pipe diameter and wall thickness, pump speed and power. They studied the effect of temperature on maximum water hammer for water (as temperature affects water density and pressure) for five different temperatures: 4, 10, 15, 20 and 25 °C. They used the WaterGEMS software [38] for the modeling and simulation. This software calculates the water density and pressure of water for set temperatures. They concluded that for 5 °C increase in temperature, the wave velocity increases by about 8 m/s. By applying this estimation to the model, it is seen that maximum water hammer increases by about 2 m of water column. Nevertheless, they did not account for different temperatures for supply and return lines and thus have not researched that effect.

Others that discussed the effect of temperature on water hammer phenomena are Dudlik et al. [39] and Saidani et al. [40], although both focus mainly on condensation hammer. Dudlik et al. [39] discussed the effect of temperature on water hammer phenomena, particularly in the context of experiments conducted at the Fraunhofer UMSICHT test rig. They concluded that the system temperature significantly affects the peaks and frequency of pressure surges throughout the system. Also, increasing the system pressure along with temperature leads to more vigorous collapse of the cavitation bubbles, causing higher pressure peaks. For example, raising the vessel pressure from 1 bar to 10 bar resulted in an increase of the first peak collapse pressure from 40 bar to approximately 58 bar.

Saidani et al. [40] discussed the impact of temperature on water hammer phenomena in copper pipe systems. They investigated the influence of temperature on water hammer phenomena for flows in a piping system with and without cavitation. Their study highlights that both wave speed and pressure head attenuation during water hammer events are temperature-dependent. Unlike steady-state flow conditions, where viscosity is the primary consideration, the bulk modulus becomes a crucial factor in transient flow, directly affecting wave amplitude and frequency. They also investigated the impact of temperature on cavitation inception and the severity of cavitation events, which are responsible for generating intense pressure peaks upon collapse. The total volume and duration of cavities increase with temperature. The

paper indicates that short-duration pressure peaks are more intense after the first pressure zone and increase significantly with temperature. In addition to heavier loadings on the pipe structure, this results also in significant dissipation of hydraulic energy in a transient flow with cavitation at higher temperatures. Finally, they noted that discrepancies between results obtained with different models suggest that further improvements are needed for better predictions at higher temperatures.

These findings highlight the complex relationship between temperature, pressure, and fluid–structure interaction in water hammer phenomena. The sensitivity of water hammer to system temperature indicates that temperature must be a key consideration in the design analysis of hydraulic systems, particularly those operating under varying thermal conditions. This underscores the critical importance of accounting for temperature effects in the analysis and design of hydraulic systems to reduce water hammer and mitigate the risk of associated damages.

2.1. Water hammer phenomena

To understand the effect of temperature on water hammer phenomena, we need to know what parameters are affecting water hammer in pipeline systems of different materials. The water hammer equations describe the acoustic behavior of weakly compressible low-Mach number flows in elastic pipes of circular cross-section. We assume here pipes of which their wall behave in a linearly elastic matter [4]. We also assume that cavitation, trapped air pockets, leakages, blockages, and fluid–structure interactions are absent. Under these assumptions, the water hammer equations for one-dimensional (1D) transient isothermal flow in horizontal pipes can be expressed in terms of head H in m and discharge Q in m^3/s by two hyperbolic partial differential equations. The continuity equation is defined by

$$\frac{\partial H}{\partial t} + \frac{c^2}{gA} \frac{\partial Q}{\partial s} = 0 \quad (1)$$

and the momentum equation is defined by

$$\frac{\partial H}{\partial s} + \frac{1}{gA} \frac{\partial Q}{\partial t} + f \frac{Q|Q|}{2gDA^2} = 0 \quad (2)$$

where A is the cross-sectional flow area in m^2 , g is the gravitational acceleration in m/s^2 , t is time in s and x is axial distance in m. The last term on the left-hand side of Eq. (2) is the quasi-static relation for the frictional head loss in m. c is the wave speed in m/s given by

$$c = \sqrt{\frac{K}{\rho_f \left(1 + \frac{D}{e} \frac{K}{E} \psi\right)}} \quad (3)$$

where ρ_f is the mass density of the fluid flowing through the pipe in kg/m^3 , K is the bulk modulus of elasticity of the fluid in Pa, E is the Young's modulus of elasticity of the pipe-wall material in Pa, D is the internal pipe diameter in m, e is the pipe wall thickness in m and ψ is the axial pipe constraint parameter.

These equations show that the evolution of the pressure head during a transient event depends on the wave speed. According to Eq. (3), the velocity of pressure wave propagation is a function of five parameters: $c = f(\rho_f, K, E, D, e, \psi)$. Of these parameters, the fluid density and bulk modulus are physical fluid properties, the Young's modulus is material property of the pipe and the inner diameter and thickness are pipe geometrical properties. This is also concluded by Urbanowicz et al. who described the parameters affecting water hammer in pipelines made of different materials, namely metal [41] and plastic [42]. They conducted numerical simulations, varying each parameter individually for an assumed deviation. In addition to the five parameters discussed here, they also considered the impact of kinematic viscosity on pressure wave propagation. However, their results indicated that, among all the parameters analyzed, only this factor does not affect pressure wave propagation. This is because it appears solely in the formulas for modeling the hydraulic resistance of the flowing liquid. However, Urbanowicz et al. did not discuss how temperature affects these parameters and consequently the water hammer phenomena. We will do that in the next subsection.

2.2. The effect of temperature on the wave speed

To understand the effect of temperature on the wave speed, it is of interest which physical fluid and pipe material parameters in Eq. (3) depend on temperature. We focus here on the physical parameters and not the thermal expansion of pipes at higher temperatures.

- The density of the fluid ρ_f . As a fluid is heated, its molecules move faster and tend to move further apart, causing the fluid to expand. This increase in volume leads to a decrease in density [43].
- The bulk modulus of the fluid K . This is a material property characterizing the compressibility of a fluid. In other words, how easy a unit volume of a fluid can be changed when changing the pressure working upon it. The bulk modulus can be defined by

$$K = -dp/(dV/V_0)$$

where dp represents the infinitesimal change in pressure, dV represents the infinitesimal change in volume and V_0 is the original volume of the material before any pressure is applied. A change in temperature causes the molecules in the fluid to move further apart, reducing the material's resistance to compression [44].

- The Young's modulus of the pipe material E . The Young's modulus varies with temperature due to changes in the inter-atomic bonding of the atoms. As the temperature increases, the Young's modulus generally decreases, which can be described by the relationship [45]

$$E(T) = E_0 e^{-aT}$$

where E_0 the reference Young's modulus at a baseline temperature (often room temperature or another specified reference point) and a the material-specific constant that describes how the Young's modulus changes with temperature T .

The density and bulk modulus are physical properties of water that affect the wave speed of pipes. Fig. 3 shows how these parameters change as function of temperature. The density of liquid water decreases almost linearly when temperature increases between 20 and 100 °C. As the wave speed scales with $1/\sqrt{\rho_f}$ it would indicate that the wave speed increases as temperature increases.

On the other hand, the effect of temperature on the bulk modulus is more complex. For water at 1 bar, the bulk modulus reaches its maximum around 50 °C. Since the bulk modulus appears in the numerator of the wave speed formula, an increase in the bulk modulus leads to an increase in wave speed, while a decrease results in a reduction. Therefore, up to approximately 50 °C, both the density and bulk modulus contribute to an increase in wave speed. However, at higher temperatures, the density and bulk modulus of water have opposing effects on the wave speed.

Other than the physical properties of water that affect the wave speed, there are also pipe material, physical and geometrical properties that affect the wave speed. Typical materials used for pipelines in district heating networks are steel or copper pipes insulated with rigid PUR (polyurethane) foam protected by an outer jacket made from PE-HD. However, the PUR and PE jacket have no effect on the pipe stiffness and thus also not on the wave speed. Thus, we have to account for the properties of the carrier pipe only. On the other hand, pipes operated at lower temperature can be made of PE, such as HDPE. Fig. 4 show the approximate bandwidth in wave speed for water filled pipelines for different pipe materials, among which steel and HDPE, and dimensions.

To determine how the physical properties of pipe materials affect the wave speed for different temperatures, we consider two speeds that determine the wave speed of a pipe: the speed of sound in water and the propagation of disturbances in elastic cylindrical tubes. The speed of sound in water can be determined by

$$c_{water} = \sqrt{\frac{K}{\rho_f}} \quad (4)$$

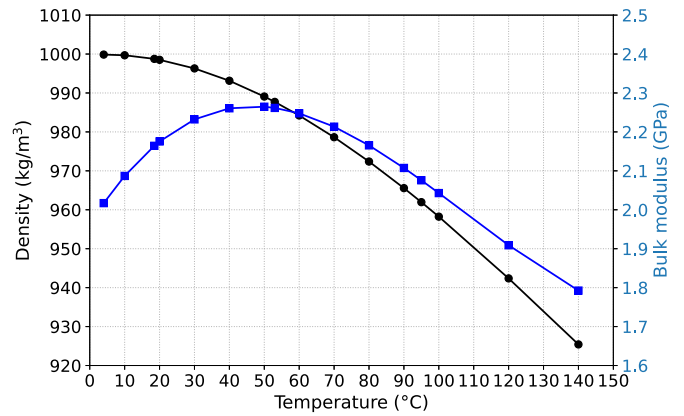


Fig. 3. The density and bulk modulus of water at 1 bar as function of temperature.

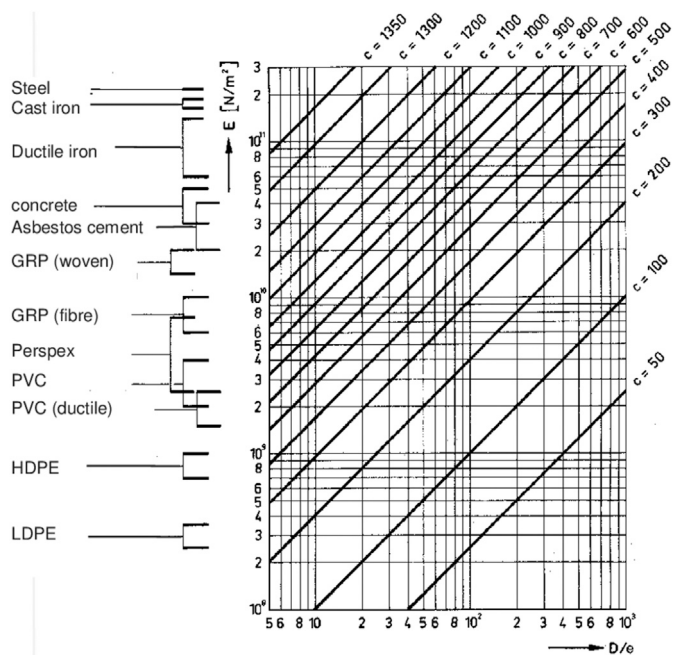


Fig. 4. Acoustic wave speed in water filled pipelines at room temperature in relation to pipe material elastic modulus E and inner diameter/wall thickness D/e ratios [46].

and the propagation of disturbances in elastic cylindrical tubes given by Résal's formula

$$c_{Resal} = \sqrt{\frac{E}{\rho_f} \frac{e}{D}} \quad (5)$$

Both contribute to the wave speed of pipes, c , by combining the stiffness terms as two springs in series, resulting in Korteweg's equation

$$\frac{1}{c^2} = \frac{1}{c_{water}^2} + \frac{1}{c_{Resal}^2} \quad (6)$$

For $\psi = 1.0$, this results in Eq. (3). Fig. 5 shows how these speeds contribute to the wave speed of a pipe for carbon steel [47] and HDPE [48]. We only consider temperatures up to 80 °C for HDPE pipes for which we found data in literature. For all material counts that the lower the Young's modulus the lower the waves speed. Note that the Young's modulus is about 100 times higher for steel than for plastic and the Young's modulus decreases about linearly with increasing temperature. In contrary for HDPE, the Young's modulus behaves asymptotically for higher temperature.

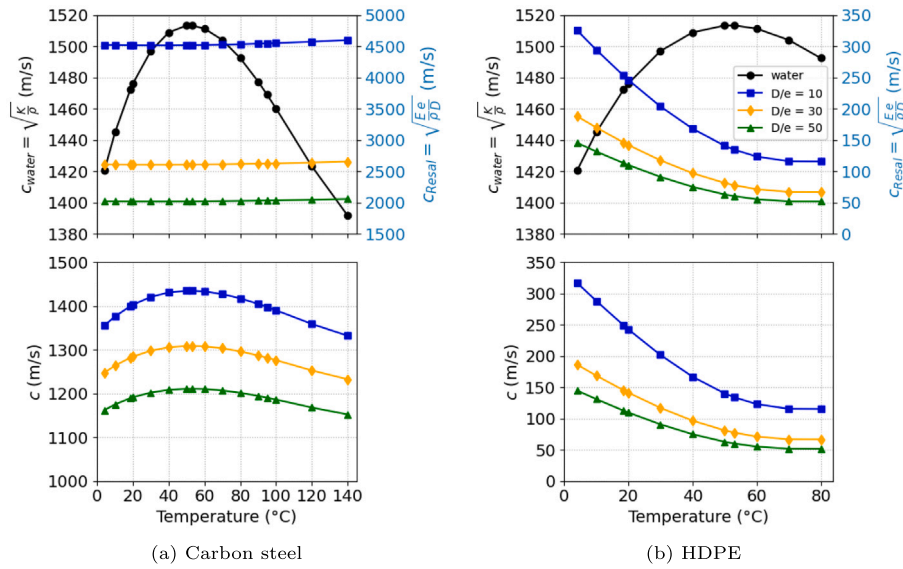


Fig. 5. (Top) two speeds that contribute to the wave speed of a pipe as function of temperature: the speed of sound in water and the propagation of disturbances in elastic cylindrical tubes as determined by the Résal formulation. (Bottom) the wave speed of a pipe determined by the Korteweg formula as function of temperature for $D/e = 10, 30$ and 50. (Left) carbon steel and (right) HDPE.

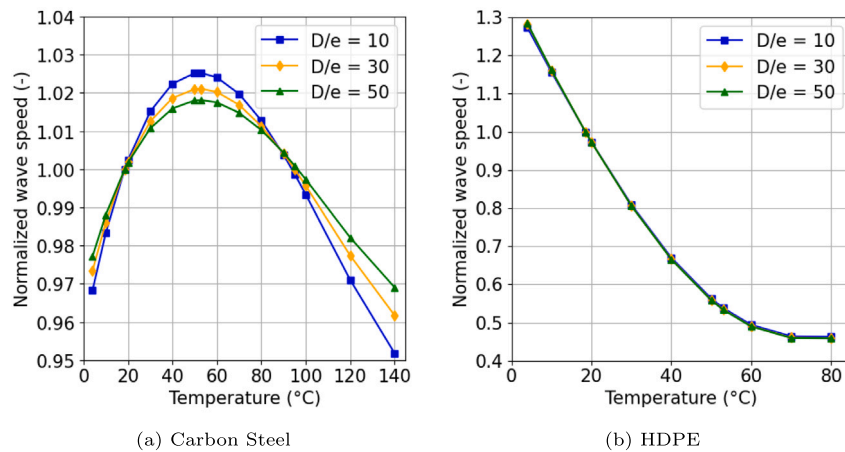


Fig. 6. The wave speed of a pipe of different materials as function of temperature for $D/e = 10, 30$ and 50 normalized with the wave speed at 18.5 °C.

Next, we examine how the pipe dimensions (geometrical parameters) affect the wave speed. Fig. 5 shows that a larger ratio of D/e results in a lower wave speed. While the trend of temperature affecting the wave speed remains consistent, the curve flattens with an increasing diameter-to-wall thickness ratio, making the effect less pronounced. To illustrate this, we plotted the wave speed normalized to the wave speed at 18.5 °C in Fig. 6. Room temperature of about this temperature is typically considered when modeling and simulating flows without accounting for temperature variations. For the HDPE pipes, the figure also shows that the D/e ratio has a negligible effect on the normalized wave speed. This is due to the dominant elasticity of the pipe material compared to the “stiff” liquid bulk modulus as shown in Eq. (3).

In conclusion, when the stiffness of the pipe is an order of magnitude lower than that of the liquid (i.e. the bulk modulus), due to either a low Young’s modulus or a high D/e ratio, the wave speed becomes dominated by the pipe. Consequently, the influence of the bulk modulus becomes negligible.

Based on these physical parameters for both the fluid and the pipe material, the trend of how temperature affects wave speed is clear. For steel pipes, the wave speed increases with increasing temperature up to a temperature of about 50 °C. It decreases again for higher

temperatures. Most steel pipes are used for applications with a return temperature around or above 50 °C, e.g. 120/80 °C for conventional high temperature (HT)-networks, 100/60 °C for HT-networks with optimized operation, 80/50 °C for (primary) transmission systems and 70/40 °C for secondary distribution networks (see also Fig. 1). Especially for the 70/40 °C networks the difference in wave speed between supply and return line is small.

The trend is different for plastic pipes. For these pipes, the wave speed decreases with increasing temperature, especially below 50 °C. This is most relevant for low and ultra-low temperature DH, which are more often made of plastic pipes [49]. Fig. 7 illustrates these trends, showing the absolute difference in wave speed between supply and return temperatures in 142 MT and HT Swedish district heating systems, assuming the pipes are made of either steel or HDPE. Note, however, that when considering relative pressures instead of absolute pressures, the differences are larger for plastic pipes than for steel pipes.

Thus, even under all assumptions, it remains difficult to determine the wave speed of a pipe in a district heating network at a certain temperature. Here we have used a Young’s modulus relation, but as Fig. 4 shows, it is not an exact value but a range for different materials. Also the inner diameter and wall thickness of the pipes are critical

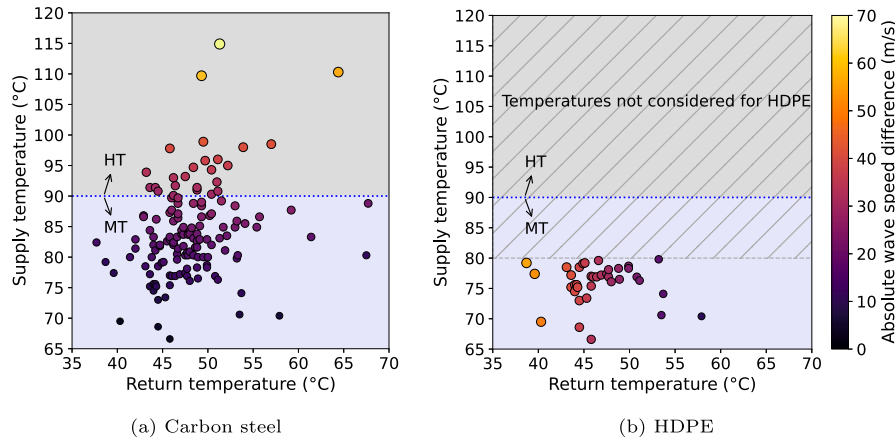


Fig. 7. Absolute wave speed difference between supply and return temperatures in 142 Swedish district heating systems from 2004 to 2010 [50] for an assumed diameter/wall thickness ratio of 10. Each dot represents one district heating system. MT = Medium Temperature networks, HT = High Temperature networks. (Left) assuming steel pipes and (right) assuming HDPE pipes.

parameters. Small measurement errors or assumptions about these dimensions can result in considerable uncertainties in the wave speed and pressure calculations. The same applies to the measurement or estimation of the fluid properties.

It is thus of utmost importance to not only account for temperature, but to also perform an uncertainty quantification for transient wave propagation in pressurized pipes for the different parameters as they may vary in a large interval [51]. Also performing measurements to determine the wave speed for different pipes is needed as literature is not extensive on this.

Finally, we stated at the beginning of this section that we assume the absence of cavitation and trapped air pockets. However, literature [52] indicates that the presence of entrained air or free gas reduces wave speed and, consequently, pressure transients. Therefore, the effect of these and other fluid impurities combined with varying temperatures require further investigation.

3. Water hammer software Wanda

Abdeldayem et al. [53] investigated several commercial software tools for the simulation of hydraulic transients and the design of hydraulic systems. They found 21 available water hammer commercial computer codes of which the majority (13 out of 21) use the methods of characteristics (MoC) to solve the hydraulic equations. Moreover, 18 out of the 21 software depend on steady/quasi-steady friction models for the computation of the water hammer equations. For the study in this paper, we use one of these codes, namely Wanda which is developed and released by Deltares. Wanda consists of different modules. The modules relevant to investigate the effect of temperature on water hammer are the Wanda Liquid module and the Wanda Heat module. The components available for each module allow for adaptable models, making it a versatile tool for various hydraulic and thermal analyses.

In this section, we explain briefly some of the differences between the models. However, we refer to the Wanda manual [54] for more detailed information about the Wanda software and to [55,56] for validation reports on the software.

3.1. Fluid and material properties

Wanda Liquid does not account for temperatures and is thus a dynamic hydraulic module. The user can specify fluid properties that remain constant during a transient simulation [54]. The default properties for water are density $\rho_f = 1000 \text{ kg/m}^3$, vapor pressure $p_v = 0.01707 \text{ bar}$, kinematic viscosity $\nu = 1 \text{e-}6 \text{ m}^2/\text{s}$ and bulk modulus $K = 2.1 \text{e}9 \text{ N/m}^2$. It is important to note that these values have associated

Table 3

Default Wanda Heat fluid properties for water [54]. c_p is the specific heat capacity at constant pressure and k is the thermal conductivity.

T (°C)	ρ_f (kg/m ³)	ν (m ² /s)	p_v (bar a)	c_p (J/kg K)	k (W/m K)
4	1000.0	1.569e-06	0.00813	4205	0.562
10	999.8	1.308e-06	0.01227	4192	0.577
18.5	998.5	1.030e-06	0.02270	4183	0.600
20	998.3	1.005e-06	0.02337	4182	0.602
30	995.7	8.014e-07	0.04242	4178	0.622
50	988.0	5.536e-07	0.12340	4181	0.641
53	987.5	5.451e-07	0.13020	4181	0.642
60	983.1	4.750e-07	0.19920	4185	0.651
70	977.6	4.132e-07	0.31160	4190	0.660
80	971.6	3.654e-07	0.47360	4196	0.668
90	965.1	3.264e-07	0.70110	4205	0.675
95	961.6	3.099e-07	0.84530	4210	0.679

uncertainties. These uncertainties can arise from various factors, including measurement precision, temperature variations (as shown in Section 2.2) and the purity of the water. Additionally, at the system level, uncertainties are often much more complex for real pipeline systems compared to lab experiments. Factors such as valve and pump activities and pipe geometry might be unknown or imprecisely known [51].

On the other hand, Wanda Heat accounts for temperature dependent properties for density ρ_f , kinematic viscosity ν , vapor pressure p_v , specific heat c_p and thermal conductivity k for the working fluid. Only the bulk modulus does not depend on temperature and is taken equal to value for the Wanda Liquid module. Table 3 shows the default temperature dependent properties for water in Wanda Heat.

With both modules, users have the option to either input the material properties of a water hammer pipe (Wave speed mode set to “Physical”), allowing the software to compute the wave speed, or directly specify the wave speed for the pipe (Wave speed mode set to “Specified”). This flexibility enables users to define different wave speeds for supply and return pipelines based on the (average) initial supply and return temperatures in the system. However in “Physical” mode, Wanda Heat computes the wave speed irrespective of the temperature of the fluid as it uses the same properties as Wanda Liquid uses for the same computation (so the properties independent of temperature). Thus, the speed at which a pressure wave can travel is in that case irrespective of using Wanda Liquid or Heat. Yet, higher temperature means lower densities, which results in slightly lower pressures during transient simulations (which can lead to cavitation).

3.2. Quasi-steady friction

Another difference between the two Wanda modules is that Wanda Heat assumes pressure p , mass flow rate \dot{m} and internal energy u as the dependent variables for the water hammer equations. On the other hand Wanda Liquid uses head H and discharge Q . This results in two ways to compute the losses due to friction for the modules. Wanda Liquid computes in steady-state the head loss due to viscous effect for incompressible fluid flow through a cylindrical pipe by the following Darcy–Weisbach equation [54]

$$H_0 - H_L = \frac{f L Q |Q|}{2g D A^2} \quad (7)$$

where subscript 0 means the upstream side of the pipe and subscript L the downstream side of the pipe. The dimensionless friction Darcy–Weisbach factor f depends on the wall roughness k and the Reynolds number Re .

Wanda Heat computes the pressure loss over the pipe according to

$$\frac{p_0}{\rho_f g} + z_0 - \frac{p_L}{\rho_f g} - z_L = \frac{8f}{LD^5 g \rho_f \pi^2} \dot{m} |\dot{m}| \quad (8)$$

where $\rho_f = 0.5(\rho_{f,0} + \rho_{f,L})$.

Wanda calculates the friction factor f iteratively using the by the user-specified wall roughness. Wanda includes several friction models. When the “Dynamic Friction” option is set to “Quasi-steady”, the friction factor is recalculated at every time step for all calculation points. This recalculation is based on the local flow velocity from the previous time step and the specified wall roughness of the pipe. For both Wanda Liquid and Wanda Heat, the friction factor is computed based on the Reynolds number, using the fluid properties of Wanda Liquid, and is not temperature-dependent. The Reynolds number is defined as

$$Re = \frac{4Q}{\pi D v} \quad (9)$$

Even though the friction factor is theoretically inversely proportional to the Reynolds number, for stability reasons, Wanda computes the friction factor for the laminar flow region up to $Re = 100$ independently of the Reynolds number, using

$$f = 0.64 \text{ for } 0 < Re < 100 \quad (10)$$

For Reynolds numbers between 100 and 2000, Wanda computes the friction factor inversely proportional to the Reynolds number as

$$f = 64/Re \text{ for } 100 < Re < 2000 \quad (11)$$

And finally in turbulent regime it computes it as

$$\frac{1}{\sqrt{f}} = -2.0 \log \left(\frac{k/D}{3.7} + \frac{2.51}{Re \sqrt{f}} \right) \text{ for } Re > 4000 \quad (12)$$

In the critical regime, $2000 < Re < 4000$, Wanda computes the friction factor with a linear interpolation between f calculated with Eq. (11) for $Re = 2000$ and f calculated with Eq. (12) for $Re = 4000$.

3.3. Method of characteristics

There are several numerical methods for the modeling of transient pressurized pipe flow [57]. Wanda utilizes the traditional Method of Characteristics (MoC), where the fundamental equations for a pipe are represented as a set of hyperbolic partial differential equations. We will first examine the classical MoC formulation for transient pressure pipe flow, followed by the MoC formulation for transient pipe flow with temperature variations. For the MoC formulation addressing transient pressure pipe flow, we consider head H and discharge Q as the dependent variables, similar to the approach used in Wanda Liquid and under the same assumptions as presented in Section 2.1. This leads to

the following set of continuity and momentum equations

$$\frac{\partial H}{\partial t} + \frac{c^2}{gA} \frac{\partial Q}{\partial s} = 0 \quad (13)$$

$$\frac{1}{gA} \frac{\partial Q}{\partial t} + \frac{\partial H}{\partial s} + \frac{f}{2gDA^2} Q|Q| = 0 \quad (14)$$

These equations can be combined and transformed into two sets of ordinary differential equations, called the compatibility equations, which we denote as the C^+ and C^- equations.

$$C^+ : \begin{cases} \frac{dH}{dt} + \frac{c}{gA} \frac{dQ}{dt} + \frac{fc}{2gDA^2} Q|Q| = 0 \\ \frac{ds}{dt} = +c \end{cases} \quad (15)$$

$$C^- : \begin{cases} \frac{dH}{dt} - \frac{c}{gA} \frac{dQ}{dt} - \frac{fc}{2gDA^2} Q|Q| = 0 \\ \frac{ds}{dt} = -c \end{cases} \quad (16)$$

We can solve these equations numerically using a finite difference approach. To derive the finite difference equations, we divide a pipe into equal elements of length ds and choose a time step $dt = \frac{ds}{c}$. In this way, the discretized equations can then be graphically represented by straight lines in space–time, known as characteristics, as shown in Fig. 8. To compute the discharge and head for a specific element i at the next time step $n+1$ (point P in the figure), we use the neighboring elements. If H and Q are known at element $i-1$ (point A in the figure) and element $i+1$ (point B in the figure) at the current time step n , we can integrate the equations along the characteristic lines to compute the unknown H_i^{n+1} and Q_i^{n+1} as follows

$$C^+ : \int_{i-1,n}^{i,n+1} \frac{dH}{dt} dt + \frac{c}{gA} \int_{i-1,n}^{i,n+1} \frac{dQ}{dt} dt + \frac{fc}{2gDA^2} \int_{i-1,n}^{i,n+1} Q|Q| dt = 0 \quad (17)$$

$$C^- : \int_{i+1,n}^{i,n+1} \frac{dH}{dt} dt - \frac{c}{gA} \int_{i+1,n}^{i,n+1} \frac{dQ}{dt} dt - \frac{fc}{2gDA^2} \int_{i+1,n}^{i,n+1} Q|Q| dt = 0 \quad (18)$$

The first two terms in the equations can easily be integrated. However, in the last term Q is not known a priori. A first-order approximation is used for this friction term. Integration and expressing H_i^{n+1} in terms of all other variables results in

$$C^+ : H_i^{n+1} = C_{i-1}^n - RQ_i^{n+1} \quad (19)$$

$$C^- : H_i^{n+1} = C_{i+1}^n + RQ_i^{n+1} \quad (20)$$

in which

$$C_{i-1}^n = H_{i-1}^n + RQ_{i-1}^n - SQ_{i-1}^n |Q_{i-1}^n| \quad (21)$$

$$C_{i+1}^n = H_{i+1}^n - RQ_{i+1}^n + SQ_{i+1}^n |Q_{i+1}^n| \quad (22)$$

and, for simplicity, R and S are determined by pipe and fluid properties as follows

$$R = \frac{c}{gA}; S = \frac{fc}{2gDA^2} \Delta t \quad (23)$$

with c the wave speed (see Eq. (3)) and f the friction factor in s^2/m^5 and Δt the time step. More about the computation of the friction factor in the next subsection.

The computation is executed in all internal computational points in the pipes for which it uses applied boundary conditions at start and end of the pipe.

In Wanda Heat, the transport of pressure waves are computed according to the MoC method for pipes that account for water hammer as described for Wanda Liquid. However, in Wanda Heat, the dependent variables are mass flow rate ($\dot{m} = \rho_f Q$) and pressure, instead of discharge and head. The pressure relates to the head as $p = \rho_f g(H - z)$. Following the same approach as for Wanda Liquid (Eqs. (13)–(23)), we can obtain the discretized equations

$$C^+ : p_i^{n+1} + \rho_{f,i} g z_i = C_{i-1}^n - X \dot{m}_i^{n+1} \quad (24)$$

$$C^- : p_i^{n+1} + \rho_{f,i} g z_i = C_{i+1}^n + X \dot{m}_i^{n+1} \quad (25)$$

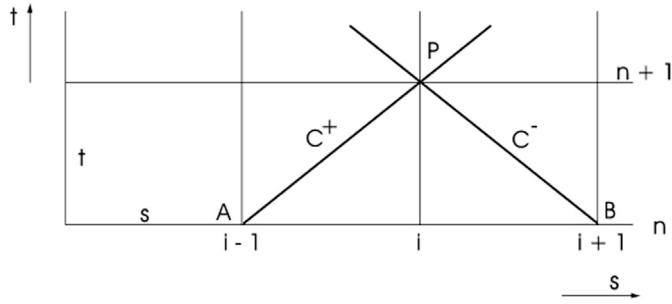


Fig. 8. MoC characteristics in the space-time plane [54].

in which

$$C_{i-1}^n = p_{i-1}^n + \rho_{f,i} g z_{i-1} + X \dot{m}_{i-1}^n - Y_i \dot{m}_{i-1}^n \left| \dot{m}_{i-1}^n \right| \quad (26)$$

$$C_{i+1}^n = p_{i+1}^n + \rho_{f,i} g z_{i+1} - X \dot{m}_{i+1}^n + Y_i \dot{m}_{i+1}^n \left| \dot{m}_{i+1}^n \right| \quad (27)$$

in which X and Y are defined by

$$X = \frac{c}{A}; Y_i = \frac{f c}{2 \rho_{f,i} D A^2} \Delta t \quad (28)$$

To determine the thermal evolution in the pipe, Wanda Heat assumes the following energy balance

$$\rho_f \frac{du}{dt} + \frac{1}{A} \frac{d(\dot{m}u)}{ds} - \frac{\beta f}{2 \rho_{f,i} D A^3} (\dot{m})^2 |\dot{m}| - q_{loss} = 0 \quad (29)$$

where $u = u(T)$ is the internal energy as function of temperature T . Furthermore, the third term on the left-hand side represents the heat loss due to friction where β is the fraction of friction converted to heat loss. q_{loss} includes all other heat losses per unit volume.

In transient mode, Wanda Heat uses for the computation of the heat transfer through the pipe the same MoC grid as for the water hammer computation with equal elements of length Δs that have a volume V . It solves at the beginning of a time step for the compatibility equations described by Eqs. (24)–(28) and at the end of a time step the discretized energy balance. In the case of positive flow, so flow from element $i-1$ to element i , the following is solved

$$\frac{V (\rho_{f,i} u_i)^{n+1} - V (\rho_{f,i} u_i)^n}{\Delta t} = (\dot{m}u)_i^n - (\dot{m}u)_{i-1}^n + \frac{\beta f (\dot{m}_i^n)^2 |\dot{m}_i^n|}{2 \rho_{f,i}^2 D A_i^2} \Delta s - Q_{loss} \quad (30)$$

where Q_{loss} represents all heat losses excluding those caused by friction.

3.4. Specified vs. adapted model wave speeds

When applying the Method of Characteristics (MoC) for numerical simulations of pipes, the wave speed used in the MoC grid (adapted wave speed c_{adapt}) can deviate from the specified wave speed (c_{spec} , based on pipe material and fluid properties or user input). This deviation occurs because the MoC grid is discrete, while the actual wave speed is continuous. In other words, the MoC requires an integer number of internal cells. Consequently, the wave speed in the model might need to be adapted. Fig. 9 illustrates this concept. The specified wave speed does not coincide with the MoC grid. Instead, the model uses an adapted wave speed that corresponds to the grid. This results in a deviation between the specified and adapted wave speeds.

The adapted wave speed, which corresponds to the grid, can be computed as

$$c_{adapt} = \frac{\Delta s}{\Delta t} = \frac{L/N}{\Delta t} \quad (31)$$

where N is the number of pipe elements. To match the specified and adapted wave speeds for a given pipe of length L the user can

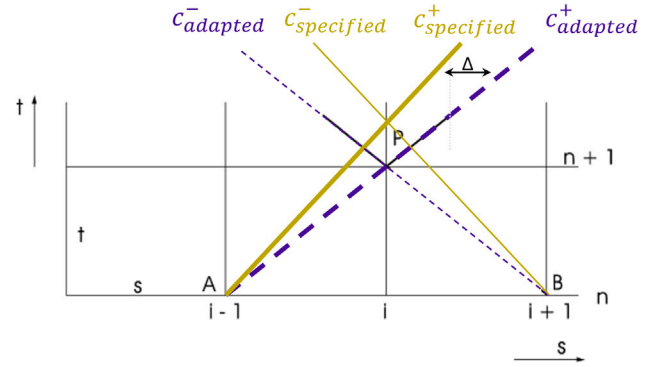


Fig. 9. MoC characteristics for specified and adapted wave speeds.

adjust the time step and/or the number of elements into which the pipe is divided. Thus, note that the discretization, specifically the grid resolution (spacing between grid points), can cause the adapted wave speed to deviate from the specified wave speed, thereby introducing errors.

3.5. Cavitation

Cavitation in pressurized pipes is a phenomenon that occurs due to changes in fluid pressure. When the local absolute pressure of a fluid drops below the temperature-dependent vapor pressure p_v , tiny voids or “bubbles”, form. These vapor bubbles travel with the fluid’s flow. When they encounter a higher pressure area, they collapse possibly with large implosion pressures. This process is known as implosion, which can damage pipeline systems.

In Wanda, cavitation is modeled as concentrated cavitation, where cavities (empty spaces in the fluid filled with vapor and/or released gas) form. These cavities can diminish over time due to higher pressures in the pipe system. When a cavity collapses, it generally causes an overpressure that travels through the pipeline. In some cases, the pressure can equal the vapor pressure over an extensive part of the pipe system. Cavitation can then occur over a relatively long section of the pipeline, where only a small part of the pipe’s cross-section is filled with vapor and gas at vapor pressure. This form of cavitation, known as extended cavitation, can occur in relatively long pipelines. Both concentrated and widespread cavities will eventually collapse and disappear. During the collapse of cavities, unallowable high pressures can occur.

Wanda does not model the transport of vapor bubbles with the fluid flow but focuses on the (de)formation of cavities and the pressure waves resulting from their collapse. When cavitation occurs at a point in the pipe within a Wanda model, this point becomes a boundary condition for the water hammer equations in the adjacent sections of the pipe. A discontinuity exists at this boundary in the spatial distribution of the discharges. The vapor volume is included in the continuity equation, and when this volume becomes zero again, the cavity collapses, and the boundary condition vanishes. This model is referred to as the Discrete Vapor Cavity Model (DVCM). The implementation in Wanda has been validated for low-temperature water applications [55].

For the MoC, this means the following. When the calculated head in a pipe element is less than the relative vapor head, it is adjusted to be equal to the relative vapor head H_v , which can be determined by

$$H_v = \frac{p_v - p_{atm}}{\rho_f g} + \frac{v^2}{2g} + z \quad (32)$$

with z the height relative to the horizontal reference plane, v the velocity and p_v the vapor pressure in the pipe element. p_{atm} is the atmospheric pressure. If this occurs, a cavity can form with a certain volume. At that location, Wanda assumes that the fluid velocity is discontinuous. The cavity disappears when its calculated volume becomes

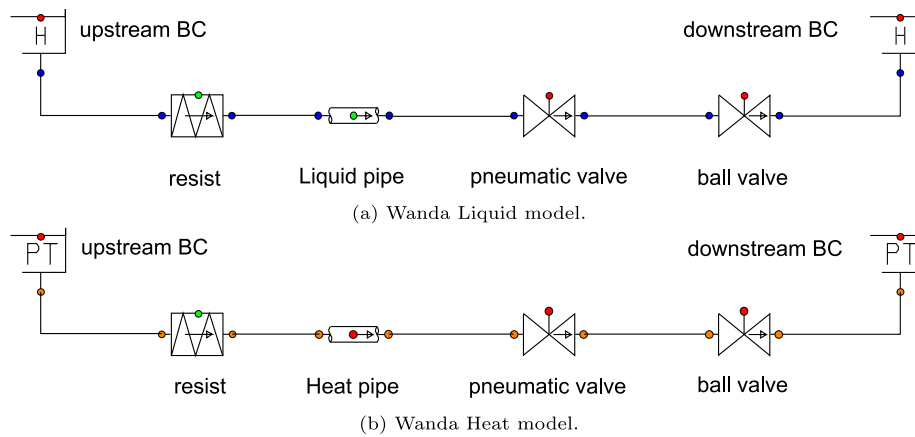


Fig. 10. Wanda models for the reference problem.

negative. To satisfy the mass balance, the last positive cavity volume is then filled with liquid. This applies when the cavitating point is an internal element point. However, when the cavitating point is at a pipe extremity (end point), it needs to be combined with the pipe's boundary conditions. We refer to the Wanda manual [54] for more details on the characteristic equations in nodal sets for the modeling of cavitation in pipes.

4. Reference problem

As highlighted in Section 2, Saidani et al. [40] conducted a comprehensive study on the impact of temperature on water hammer phenomena in a copper pipe system. Their research focused on the effects of temperature on water hammer phenomena with cavitation, considering both cavitating and non-cavitating transient flow scenarios. We consider their study as the reference problem for further investigating the impact of temperature on water hammer phenomena.

Saidani et al. [40] modeled and simulated a system that consists of a 15.22 m long copper pipe with an inner diameter of 0.02 m and a wall thickness of 1 mm. A centrifugal pump supplies the system with a nominal flow rate of 1.0 l/s and a nominal head of 46 m. In addition, the system consists of a hydro-pneumatic tank upstream of the pump and a check valve directly downstream of the pump. Finally, two quarter-turn ball valves are located at the downstream end of the pipe, with one pneumatically actuated to generate water hammer and the other manually operated to control the initial discharge.

They performed two types of simulations. The first, with a low initial velocity of 0.423 m/s, resulted in single-phase water hammer without cavitation. The second, with an initial flow velocity of 0.497 m/s, resulted in a transient flow with cavitation. Their water hammer code includes a single-phase model, a Discrete Vapor Cavity Model (DVCM), and a Discrete Gas Cavity Model (DGCM). Additionally, they used a quasi-steady friction model and two unsteady friction models: Brunone and Vardy & Brown. They compared their simulation results with the experimental results of Soares et al. [58]. While they accounted for temperature-dependent wave speeds, it is unclear how this was applied in their transient model and whether temperature was considered in other properties.

In this study, we conduct a similar analysis using Wanda 4.7. We employ two different modules: Wanda Liquid and Wanda Heat. In Wanda Liquid, we model and simulate the transient hydraulics without considering temperature dependence for any parameter, except for the wave speed of copper, which is computed based on the temperature. The fluid's density, viscosity, and bulk modulus remain constant throughout the simulations, assuming properties at 18.5 °C — the temperature at which the experiment was conducted. These properties

include a density of 998.5 kg/m³, a vapor pressure of 2.27 kPa, a kinematic viscosity of 1.07E−6 m²/s, and a bulk modulus of 2.17 GPa. Additionally, we perform simulations with Wanda Heat, which accounts for temperature-dependent variations in density, kinematic viscosity and vapor pressure.

4.1. Model setup

Fig. 10 illustrates the Wanda Liquid and Wanda Heat models. The Liquid model features a head boundary condition (BC) at both the upstream and downstream ends of the system, while the Heat model employs a pressure–temperature boundary condition on both sides. The reference model includes a tank at the upstream BC. However, we do not model the tank in Wanda as its dimensions (other than its volume of 60 l), air quantity, or initial fluid level were not specified by Saidani et al. [40]. Instead, we initialize the BCs at $H = 0$ m and $p = 0$ bar for Wanda Liquid and Wanda Heat, respectively. In both models, we use a resist component to simulate the head of 46 m provided by the pump, as the pump characteristics are not available. This approach is valid because, as in the reference, the upstream reservoir is assumed to be infinite, ensuring that the head remains constant during the short transient duration. This method also ensures that the same head is applied in both the Liquid and Heat models, eliminating the need to convert head to pressure for Wanda Heat. Furthermore, we assume a wall roughness of 0.001 mm, based on the steady-state pressure drop results of the reference problem.

We simulate the flow in the system by specifying the initial discharge for the ball valve in the model that is used to control the flow (i.e. the valve furthest downstream). For Wanda Liquid, we can specify the initial discharge for the ball valve in liters per second (l/s). In contrast, for Wanda Heat, we need to specify the mass flow rate in kilograms per second (kg/s). Therefore, we must consider the fluid density based on temperature to ensure that the initial discharge is consistent across all cases.

Furthermore, we model the closure of the other (pneumatic) valve, assuming a linear valve characteristic with the same concave closing curve as described in [40]. Eq. (33) describes the closing curve for which we apply an actual closure time t_c in 0.018 s and $m = 5$ as follows

$$\tau_v = 1 - \frac{t^m}{t_c^m} \quad (33)$$

where τ_v is directly proportional to the valve opening.

Fig. 11 shows the applied closure curve in the Wanda models, as well as in the reference problem. The figure also demonstrates that the discharge through the system during valve closure in the Wanda models corresponds to that of the reference problem.

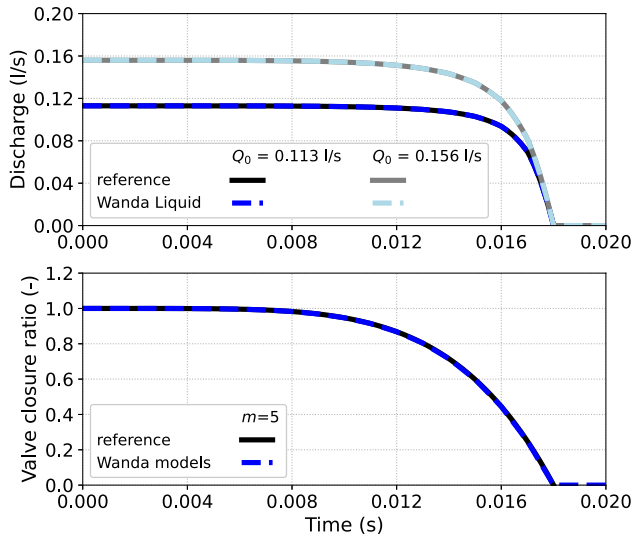


Fig. 11. (Top) discharges through the Wanda Liquid pipes during valve closure compared to the reference. (Bottom) the applied valve closure curve with $m = 5$.

Table 4
Wave speed specified and adapted in model for copper for a time step of $2.5e-4$ s.

T (°C)	c_{spec} (m/s)	c_{adapt} (m/s)	dev. (%)	n (-)
4	1222	1218	0.36	50
10	1238	1242	0.36	49
18.5	1255	1242	1.00	49
20	1257	1242	0.90	49
30	1270	1268	0.13	48
40	1278	1268	0.76	48
50	1281	1268	0.99	48
53	1281	1268	0.99	48
60	1280	1268	0.91	48
70	1276	1268	0.60	48
80	1269	1268	0.05	48
90	1260	1242	0.66	48
95	1255	1242	1.00	49

Finally, we assume the same wave speeds for copper as function of temperature as in the reference case for the water hammer pipe in the model. Table 4 summarizes the wave speeds as specified in the model. We choose a time step of $2.5e-4$ s, resulting in approximately 48 internal grid points in the pipe for the MoC grid, similar to Saidaini et al. [40]. Since the MoC requires an integer number of internal cells, as we explained in Section 3.4, the wave speed in the model needs to be adapted to the MoC grid. The adapted wave speed and the number of elements are summarized in the table, along with the deviation between the two wave speeds. Although we concluded that the wave speed varies with temperature, the model uses an adapted wave speed of $c_{adapt} = 1268$ m/s for all temperatures between 30 °C and 80 °C for the copper pipe.

To match the specified and adapted wave speed, the user needs to adjust the time step for each model according to Eq. (31) based length of the pipe and the number of internal grid points. This adjustment ensures that the time step is appropriately scaled for the given wave speed and model parameters. However, this means that a different time step will be required for the different applied temperatures. To show this, we also apply a time step of $2.527e-4$ s for the Wanda Liquid model with fluid properties at 18.5 °C, to ensure that the adapted wave speed is equal to the specified wave speed of $c = 1255$ m/s for this scenario.

4.2. Simulation scenarios

Following the approach of Saidaini et al. [40], we examine two scenarios. In the first scenario (case 1), the initial discharge is set

to $Q_0 = 0.113$ l/s, resulting in single-phase flow without cavitation throughout all simulations at various temperatures in the reference problem. In the second scenario (case 2), we repeat the simulations with an initial discharge of $Q_0 = 0.156$ l/s, which lead to transient flow with cavitation as observed in their study.

We begin by conducting steady-state simulations for both scenarios to determine the pressure drop along the pipe at temperatures of 4, 10, 18.5, 20, 30, 40, 50, 53, 60, 70, 80, 90, and 95 °C. These results are then compared with those reported by Saidaini et al. [40]. It is important to note that the pipe material properties do not influence the steady-state results.

Subsequently, we perform transient simulations for both scenarios, analyzing only the first 10 pressure oscillations (0.5 s) from the moment the valve closes, during which the tank will not have time to react. We verified this through simulations with different tank dimensions and properties.

As explained in the previous section, the chosen time step affects whether the adapted wave speed for the MoC grid matches the specified wave speed or if there is a deviation. To study this, we compare the Wanda Liquid results, with fluid properties at 18.5 °C, against the flow results of the reference model with their quasi-steady friction model for two different time steps.

The first time step is the general time step of $2.500e-4$ s, chosen for all simulations in this study, which results in an adapted wave speed c_{adapt} of 1242 m/s (see Table 4 for this scenario). The second time step is $2.527e-4$ s, chosen to ensure that the adapted wave speed matches the specified wave speed of $c = c_{spec} = 1255$ m/s for this scenario.

4.3. Steady-state results

We begin with steady-state simulations for the two cases, where the pressure head along the pipe drops due to friction. Fig. 12 illustrates the pressure difference along the pipe at various temperatures. The results obtained using Wanda Heat align closely with the reference results. In these simulations, the pressure drop decreases with increasing temperature due to the reduction in density, which in turn lowers the viscous forces. For Wanda Liquid, we assumed a constant density corresponding to 18.5 °C for all simulations. Since the density is independent of temperature, the pressure drop remains constant.

It is important to note that while Wanda Heat accounts for temperature in the head loss equation (Eq. (8)), it uses temperature-independent parameters for calculating the Reynolds number (Eq. (9)). The Reynolds number is then used to compute the friction factor using the Colebrook-White equation (Eq. (12)). At 90 °C, the Reynolds number is approximately three times higher than at room temperature for the cases presented. This could affect the pressure drop. We do not know to which extent the Reynolds dependency is accounted for in the reference model.

4.4. Transient results

For the transient simulations, we close the valve in 18 ms as described at the beginning of this chapter. The simulation time is 0.5 s, such that we capture the first 10 pressure oscillations. We apply the temperature dependent wave speed to the Wanda Liquid and Wanda Heat pipes. Thus even though we do not account for temperature in Wanda Liquid, we can see how adjusting the wave speed affects the pressure head in the system compared to the standard conditions at room temperature (18.5 °C in the reference problem).

First, we perform the same simulations as reference case 1 with $Q_0 = 0.113$ l/s for 18.5 °C for two different time steps. We compare the results with those performed with the Quasi-steady friction solver in the reference problem. Fig. 13 shows the comparison.

For the time step of $2.527e-4$ s, the adapted model wave speed is equal to the specified wave speed of 1255 m/s. The Wanda Liquid simulation results for this time step correspond to those of the reference.

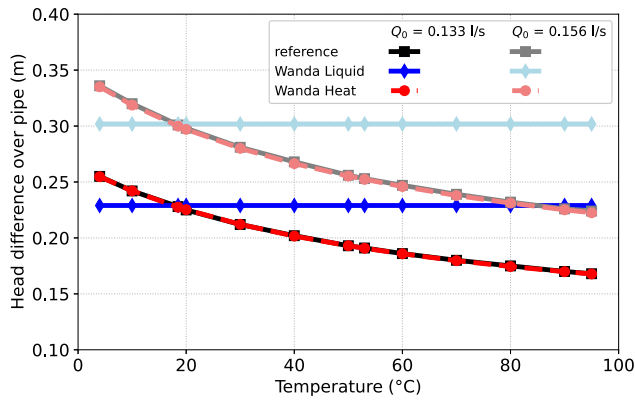


Fig. 12. Temperature effect on the pressure difference over the copper pipe for two initial discharges. Comparison between Wanda steady-state simulation results and the reference.

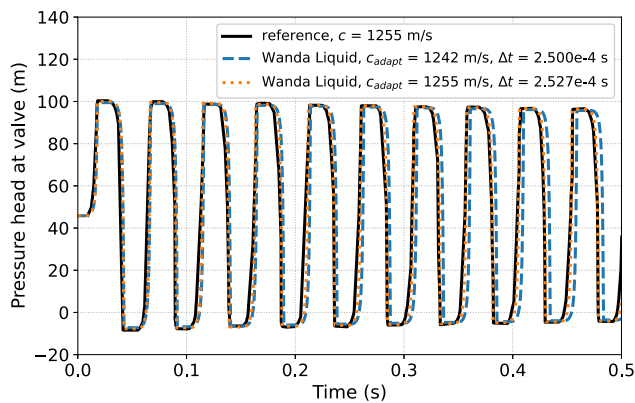


Fig. 13. Case 1: Comparison between single-phase flow results of Saidani et al. [40] using a quasi-steady friction model and the results from Wanda Liquid at 18.5 °C with a specified wave speed c of 1255 m/s for the pipe, evaluated for two different time steps.

However, for the time step of 2.500×10^{-4} s the adapted wave speed of 1242 m/s is smaller than the specified wave speed of 1255 m/s, which results in an increasing delay over time compared to the reference. Also, the wave amplitude is slightly less in the latter case, as this directly relates to the wave speed. Overall, the Wanda simulation results correspond well with the reference results for the Quasi steady friction model.

For reference case 1 with $Q_0 = 0.113$ l/s, all simulations performed by Saidani et al. [40] for different temperatures resulted in single-phase flow transients without cavitation. Fig. 14 shows the results of our simulations for a copper pipe performed with Wanda Liquid and Wanda Heat for temperatures 4, 18.5, 53, and 95 °C. Similar to the reference, the transients are single-phase flow transients. The quasi-steady friction model correctly estimates the peak in the first pressure zone, as observed in the experiment by Soares et al. [58], but does not accurately describe the attenuation of the pressure head. This is also what Saidani et al. [40] concluded about their implemented quasi-steady friction model. The results for $T = 18.5$ and 53 °C fully overlap. This is expected as the adapted wave speed is exactly the same as Table 4 shows. There is a notable shift in phase and attenuation, increasing in time, due to the reflection of the wave on the closed valve and upstream boundary condition.

What is striking, compared to the results of Saidani et al. [40], is that our simulations with Wanda Heat at 95 °C resulted in a transient flow with pressure spikes due to the collapse of cavitation bubbles, as shown in Fig. 14. Cavitation begins to occur at temperatures from 70 °C. This is expected because higher temperatures lead to higher vapor pressures, making it easier to reach the vapor pressure when pressure drops during a transient event. At 95 °C, the vapor pressure is 0.85 bara, while at 18.5 °C, it is 0.020 bara [54]. The reference results also show pressure drops to the vapor pressure, but since they only used a single-phase flow solver without cavitation model for case 1, cavitation did not occur in their case.

Next, we repeat the simulations for an initial discharge of $Q_0 = 0.156$ l/s which resulted in transient flows with cavitation in the simulations performed by Saidani et al. [40]. Fig. 15 shows the computed pressure head at the valve over time with Wanda Liquid and Wanda Heat. The pressure peaks in the second and third pressure zones are between 40 and 70 m higher predicted with Wanda than with the model of Saidani et al. [40]. A big difference in case 2 is the use of a quasi-steady friction model in Wanda, compared to the unsteady friction models used by Saidani et al. [40]. The quasi-steady friction model causes the pressure to drop to the vapor pressure more frequently and for longer durations. This results in cavitation and subsequent pressure peaks due to cavitation implosion.

Even though the adapted wave speed is 1242 m/s for both $T = 18.5$ and 95 °C, the cavitation behavior differs at these temperatures due to differences in vapor pressure. This also leads, at higher temperatures, to more vigorous collapse of the cavitation bubbles, causing higher pressure peaks.

5. Practical problem

As a practical example, we examine the study by Paananen and Henttonen [33], which modeled a 1000 MW heat transport system for district heating in Helsinki. The system includes a hot supply line and a cold return line to transport heat produced at the Loviisa Nuclear Power Plant (NPP) to the city. Both lines consist of a 77 km steel pipeline with an inner diameter of 1200 mm and a 100 mm thick insulation layer. The circuit includes four pumping stations: three with pumps on both lines and one with a pump only on the cold return line, totaling seven identical pumps operating at the same speed. Although their study does not mention wave speeds, we derived a wave speed of 1600 m/s for the steel pipes in both the hot supply line and the cold return line from their plotted results. This value is slightly rounded up compared to what is practically possible, as the speed of sound in water at typical temperatures and pressures of heating networks is below this value.

Paananen and Henttonen [33] conducted three types of simulations to analyze the system behavior: tripping of a single pump, tripping of a pair of pumps in the same pumping station and the simultaneous tripping of all pumps. Their results showed tripping a pair of pumps caused worse pressure spikes than tripping a single pump. However, simultaneous tripping of all pumps did not cause any high or low pressure peaks.

In this study, we replicate their model using the Wanda Heat module. Similar to their approach, we analyze the effects of a single pump trip and the simultaneous tripping of a pair of pumps in one pumping station, focusing on the pressure peaks in the system. Additionally, we introduce temperature-dependent wave speeds for the pipes and the effect of that on the system behavior.

5.1. Model setup

Fig. 16 depicts the setup of the Wanda Heat model. We constructed the model using the available information from the article, but due to incomplete data, we made several assumptions. Specifically, we used the default temperature-dependent fluid properties of Wanda as described in Section 3.1 and estimated the pump and pipeline parameters

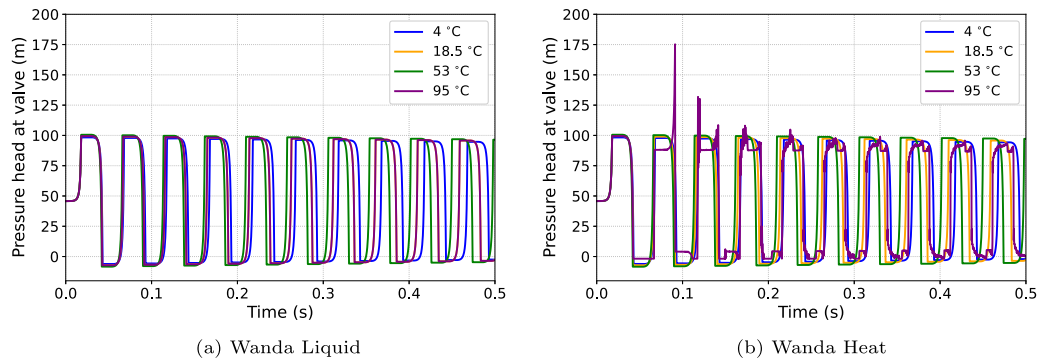


Fig. 14. Case 1: Wanda transient simulation results for fluid temperatures of 4, 18.5, 53 and 95 °C in the copper pipe system.

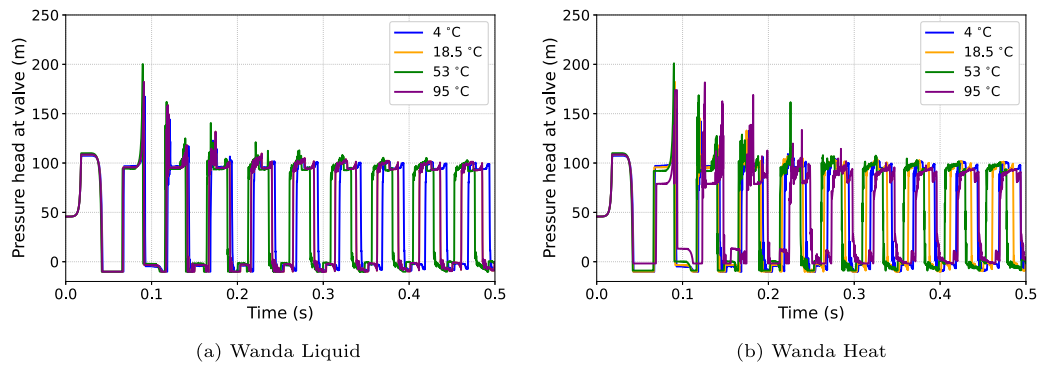


Fig. 15. Case 2: Wanda transient simulation results for 4, 18.5, 53 and 95 °C for a copper pipe.

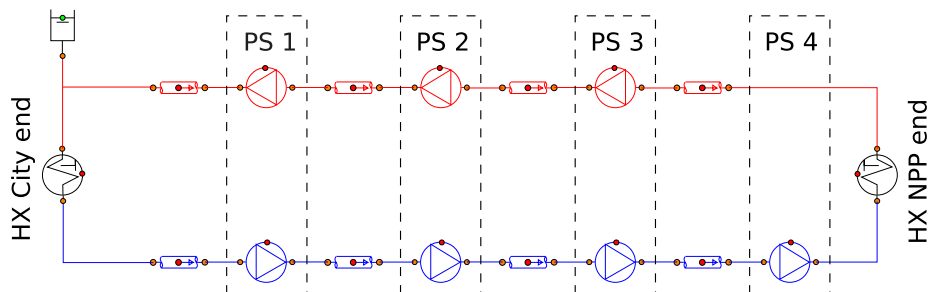


Fig. 16. Wanda Heat model for the practical problem. In red the hot supply line between the Nuclear Power Plant (NPP) and the city.

to align our results with theirs. Additionally, we did not consider the pipeline elevation profile, as the hydrostatic pressure was subtracted from the pressure profiles of their main results.

We model the 77 km long supply and return pipelines with an inner diameter of 1.2 m and assumed D/e ratio of 10. Based on the steady-state results presented by Paananen and Henttonen [33], we assume a wall roughness of 0.15 mm for the pipes.

Since the pump characteristics are not included in the reference publication, we estimated their characteristics and operating speeds by using the affinity rules for pumps to calibrate the model based on the reported results. Fig. 17 shows the applied pump curves for all pumps in the Wanda Heat model. The pumps have a rated speed of 1485 rpm and an assumed polar moment of inertia of 300 kg m². With an initial pump speed of 1356 rpm for all running pumps, we ensure the same discharges for the hot and cold lines as reported by Paananen and Henttonen [33]. These are 3.79 m³/s and 3.63 m³/s, respectively, for the hot supply line of 120 °C and the cold return line of 54 °C.

The model also includes a heat accumulator at the side of the city to store heat from the network. We model the accumulator as a surge tower which is open to the atmosphere at the top with an area of 1000 m² and infinite height to accommodate for the 50,000 m³ as included

in their model. Also, the area is sufficiently large that the variation in the fluid level in the accumulator will be negligible for short transients.

Furthermore, the model includes heat exchanger (HX) components on the points where the supply and return lines connect. These HX components determine the supply (120 °C) and return (54 °C) temperatures in the direction of the flow to the respective lines. Downstream of the HX at the city end, we set a pressure of 9.74 bar, while upstream of the HX at the NPP end, we set a pressure of 17.55 bar. We estimated these pressures based on the steady-state results plotted by Paananen and Henttonen [33], ensuring that the systems' pressure is well-defined. Note that we do not account for pressure losses across the heat exchangers.

Finally, we did not account for any heat losses in the Wanda Heat model because the insulation properties and the temperature decrease along the pipes are unknown. Additionally, we expect only small temperature variations due to losses, as the pipes are insulated with a 100 mm thick layer of insulation.

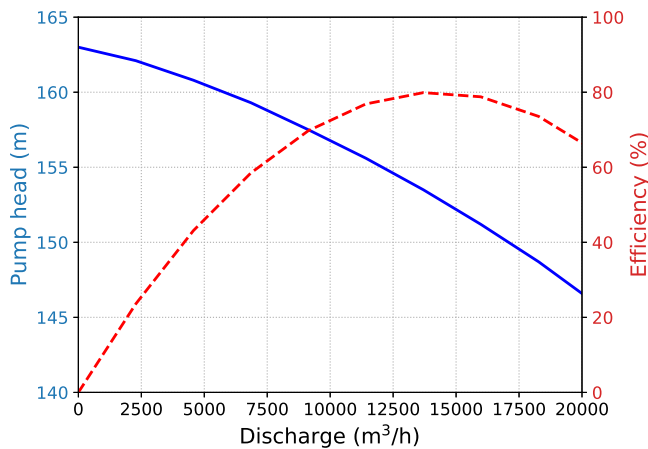


Fig. 17. Pump curve for all pumps in the Wanda Heat model.

5.2. Simulation scenarios

Following the approach of Paananen and Henttonen [33], we examine two transient scenarios: a single pump trip and the tripping of a pair of pumps.

The first scenario involves a single pump trip in the supply line at the second pumping station, viewed from the city. We use this scenario to compare our Wanda Heat model results with their study. Initially, we perform a steady-state simulation with all pumps running to compare the pressure losses across the system. Next, we simulate the tripping of the pump in the supply line. We perform this transient simulation with a time step of 10 ms, as used by Paananen and Henttonen [33], with the pump tripping at 0 s of simulation time. We then analyze the first 8 s following the pump trip. This allows us to compare the pressure changes obtained with the Wanda model to their results. For this scenario, we apply a wave speed of 1600 m/s, as determined from their study, to all pipes.

For the second scenario, we simulate the tripping of a pair of pumps in the first pumping station, viewed from the city end, using the Wanda Heat model. In the first simulation, we apply a wave speed of 1600 m/s to both lines. We then compare these results with a second simulation for which we apply temperature-dependent wave speeds. We assume that the wave speed of 1600 m/s corresponds to 18.5 °C, where the normalized wave speed is 1.0 according to Fig. 6. For steel pipes with a D/e ratio of 10, this translates to a wave speed of 1550 m/s for the hot supply line and 1640 m/s for the cold return line. This approach allows us to study the impact of wave speed variations due to temperature differences on the system behavior. Also in this simulation, we use a time step of 10 ms to capture detailed changes in pressure profiles throughout the simulation.

5.3. Single pump trip results

Fig. 18 compares the pressure profiles for the steady-state simulation with all pumps running obtained with the Wanda Heat model to the results of Paananen and Henttonen [33]. The pressure results of the Wanda model correspond well, with some small deviations in terms of absolute pressure (less than 0.5 bar) and pressure gradients along the system. This may be due to different modeling of the hydraulic losses in the system. Additionally, the absence of detailed information about the system and the assumptions made may contribute to this difference. We should also note that because they subtracted the hydrostatic pressure from their pressure profiles, resulting in non-straight lines, it is challenging to extract exact data from their plots. Yet, we find the Wanda Heat model results acceptable for studying the effect of temperature-dependent wave speeds in the transient scenarios.

Next, we analyze the transient results for this scenario. Fig. 18 illustrates these results, showing the wave propagation in the supply line after 2, 4, 6, and 8 s of simulation time for both the Wanda Heat model and the results obtained by Paananen and Henttonen [33]. This comparison reveals that the amplitude of the pressure waves from the Wanda Heat model differs by up to 1 bar from the practical problem. This discrepancy could be due to insufficient information about their model. Furthermore, the results from Paananen and Henttonen [33] are coarse, with limited data points along a pipe, which could also lead to an underestimation of their wave amplitudes. Additionally, the pump component in the Paananen model might include bypasses parallel to the pumping station, which limit the pressure drop when the suction pressure exceeds the discharge pressure. However, we do not expect that the difference between the models will influence the overall behavior of the system.

5.4. Tripping of a pair of pumps results

For the second scenario, the two pumps at the first pumping station from the city end of the network trip at the beginning of the simulation. All other pumps keep running at their initial speed. In the first simulation, the wave speed is set to 1600 m/s in both lines. Fig. 19 shows the results for this simulation after 200 s, along with the steady-state results (0 s of simulation time, with all pumps running) for this scenario.

Similar to the findings of Paananen and Henttonen [33], the system reaches a new steady-state solution 200 s after the tripping of the pump pair. Following the failure event, the pressure in the system reaches extreme values. As the flow in the system decreases after the tripping of the pumps, the pump heads increase and the pressure gradients along the pipes decrease. Consequently, the pressure drops below the vapor pressure in the return line. Both our results and those of Paananen and Henttonen [33] show a pressure drop to about -6 bar, which is not physically possible. Like their study, we did not account for cavitation in this simulation. Although enabling the cavitation model in Wanda would prevent pressures from dropping below the vapor pressure, we chose not to. This allows us to analyze the water hammer phenomenon in detail without cavitation, including wave reflection, and compare our results with theirs. Consequently, both models currently underestimate this phenomenon, as cavitation bubble collapse could lead to extreme pressure spikes, as observed in Section 4.3. Therefore, accounting for cavitation in failure event simulations is essential for improving reliability.

For the second simulation, we introduce temperature-dependent wave speeds, as detailed in Fig. 6 in Section 2, and compare these results with the first simulation where the wave speed is 1600 m/s for both lines. This analysis focuses on the part of the network at the NPP end.

Fig. 20 illustrates the pressure behavior in the pipes at 38.0, 39.0, and 40.0 s of simulation time for the scenario with temperature-dependent wave speeds. It is evident that the wave in the return line propagates faster than the wave in the supply line. After 40.8 s of simulation time, the wave caused by the pump trip in the supply line, traveling at 1550 m/s, has not yet reached the end of the network. Meanwhile, the pressure wave caused by the pump trip in the return line, traveling at 1640 m/s, has already passed through the HX component at the NPP end and into the supply line. This wave interferes with the approaching wave from the supply line pump trip, causing the pressure to drop locally by about 3 bars compared to when all pumps were still running. In contrast, the waves traveling at 1600 m/s in both the supply and return lines have not interfered at all, as they have only reached the NPP end 40.8 s after the tripping of the pumps.

Fig. 21 shows the time evolution of the pressure waves at a distance of 77.57 km from the city end for both simulations. The same dip in pressure observed in Fig. 20 is visible in the supply line with the wave traveling at 1550 m/s, due to interference with the return line pressure wave. When both wave speeds are the same, higher pressures

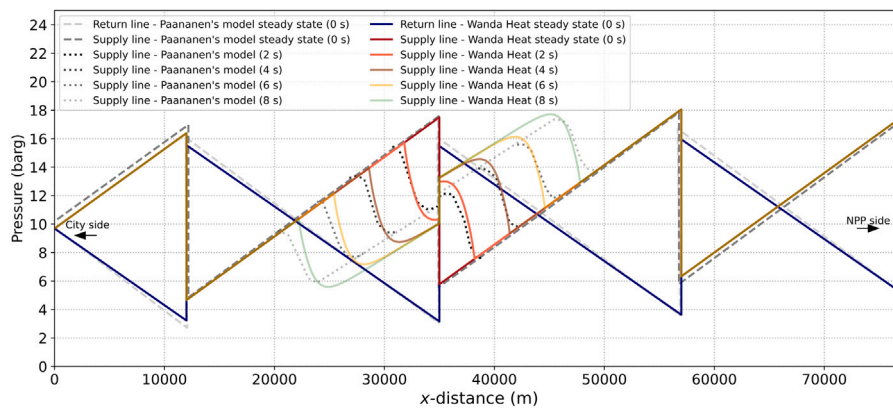


Fig. 18. Pressure profiles (dashed lines) for single pump trip scenario after 2, 4, 6, and 8 s of simulation time. Steady state pressure in solid lines as reference.

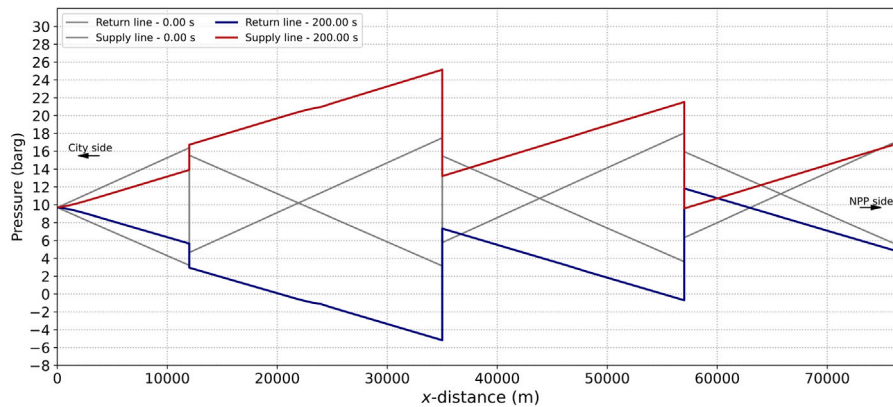


Fig. 19. Pressure profiles along the Helsinki heating transport pipelines with the supply (in red) and return lines (in blue) for the Wanda heat model, 200 s after the tripping of a pair of pumps. The steady state is included as a reference (in gray).

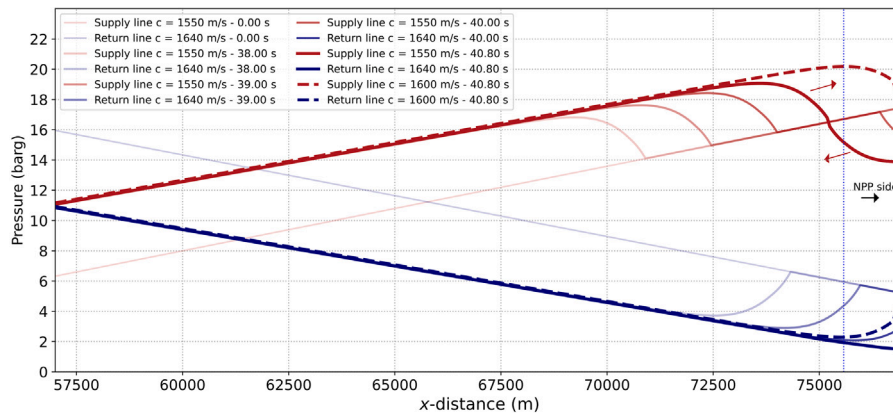


Fig. 20. Pressure throughout the simulation at the nuclear power plant end of the network for model with reference wave speed (dashed line) and temperature dependent wave speed (solid line) for both supply (in red) and return (in blue) lines for different instants during the simulation. The vertical dashed line indicates the distance of 77.57 km from the city end.

are obtained compared to the temperature-dependent wave speeds. This is because the pressure wave in the supply line has more time to develop fully to the end of the supply line without interference from the wave in the return line. As it takes longer for the wave in the supply line to reach the return line with temperature-dependent wave speeds, the period of low pressure in the return line is extended compared to when both wave speeds are 1600 m/s.

This practical case demonstrates the impact of different wave speeds due to varying supply and return temperatures within the system, which could have several implications for the overall stability and safety of the system. If the system is equipped with control elements,

near the NPP end, that continuously monitor the network's pressure levels, these elements might interpret the sudden pressure changes as an additional failure. Consequently, they could trigger protective measures, such as shutting down certain components or activating bypass valves, to prevent potential damage. While these actions are intended to be protective, they could cause additional trips or shutdowns in other interconnected components, potentially leading to cavitation. Incidental or over time, this could lead to severe failures.

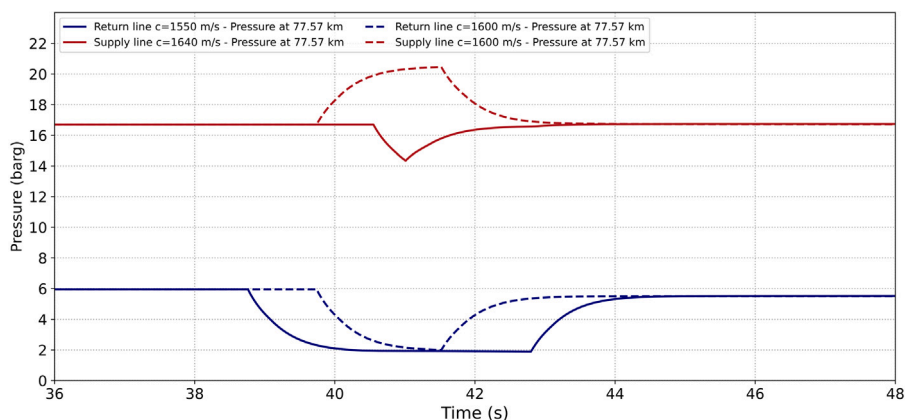


Fig. 21. Pressure over time at location 77.57 km with reference wave speed (dashed line) and temperature dependent wave speed (solid line) for both supply (in red) and return (in blue).

6. Conclusion and recommendations

Water hammer, a phenomenon characterized by sudden pressure surges in pipelines, poses significant risks to district heating systems. This study has highlighted the impact of temperature on water hammer events, emphasizing the need for comprehensive analysis and mitigation strategies during the design phase of DH transmission and distribution systems.

Different modeling approaches, including pseudo-dynamic, dynamic hydraulic, and fully dynamic thermal-hydraulic models, offer varying levels of accuracy in simulating water hammer events. The choice of model should align with the specific requirements of the DH system being analyzed.

Our study demonstrates that water hammer is impacted by the system temperature, which affects wave speed, pressure surges and cavitation. The physical and geometrical properties of pipeline materials, such as steel, copper and HDPE, play a key role in determining the severity of water hammer. The Young's modulus, which decreases with temperature, affects the wave speed and, consequently, the pressure surges. The wave speed in steel and copper pipes increases up to 50 °C before decreasing, whereas in HDPE (plastic) pipes, wave speed generally decreases with rising temperature. Typically, higher wave speeds lead to more severe water hammer effects.

To assess the impact, we modeled and simulated a reference problem involving rapid valve closure in a copper pipe system with different initial discharges, considering both cavitating and non-cavitating flow scenarios. The steady-state results show that the pressure head at the downstream end of the pipe increases with temperature due to decreasing density, independent of pipe material properties. On the other hand, the transient results reveal that higher temperatures lead to cavitation and more intense pressure peaks, which could be missed without considering thermal-hydraulic phenomena.

The analysis highlights the system's sensitivity to various factors, particularly the inclusion of temperature in models. Temperature significantly influences wave speed, pressure drop, and cavitation behavior, leading to more accurate predictions of transient flow behaviors and pressure oscillations. Additionally, the choice of friction models, whether quasi-steady or unsteady, impacts simulation outcomes, especially during cavitation events. Unlike quasi-steady models, unsteady friction models account for transient frictional losses, resulting in more accurate pressure fluctuation predictions and reduced cavitation risks. Therefore, incorporating an unsteady friction model in the Wanda software is recommended. Prior to the implementation of unsteady friction models it is important to understand the interaction between temperature and unsteady friction. Furthermore, using a cavitation model is essential at higher temperatures to capture early onset and severe cavitation events, thereby improving simulation reliability and

aiding in robust pipeline design. Additionally, ensuring the adapted wave speed matches the specified wave speed is essential for accurate simulations, though challenging in systems with pipes of varying lengths and materials.

The analysis of a 1000 MW district heating system to Helsinki, focusing on pump failures, revealed that using a single average wave speed for both supply and return lines simplifies the model but underestimates pressure peaks due to partial cancellation of reflecting waves. In contrast, applying temperature-dependent wave speeds provides more precise predictions of pressure wave propagation, pressure drops, and cavitation risks. The interaction between pressure waves in the supply and return lines creates an amplifying effect, causing significant pressure drops. Understanding these phenomena is crucial for system stability and safety, as sudden pressure changes could trigger protective measures, potentially leading to cavitation and weakening the structural integrity of the pipelines over time.

Our findings underscore the importance of incorporating temperature-dependent properties in water hammer analysis. This approach ensures more accurate predictions and helps in designing robust DH systems capable of withstanding transient events. Thus to ensure reliable heat supply, it is crucial to raise awareness about water hammer risks among designers and operators of district heating systems—especially now and in the near future as large-scale district heating networks are being developed.

Future research should focus on refining simulation models to better account for temperature effects and other dynamic factors. This includes the development and validation of cavitation models at higher temperatures to understand their impact on pipeline integrity and performance. Furthermore, the impact of dissolved air and other impurities, along with temperature effects on wave speed, should be investigated. Additionally, experimental studies are essential for validating simulation results, particularly in high-temperature scenarios and cavitation events. These studies provide data to improve existing models and enhance the reliability of water hammer predictions in district heating systems. Finally, studying the long-term effects of repeated transient events, including cavitation, on pipeline materials and joints at different temperatures can provide valuable insights into maintenance schedules and the lifespan of pipeline systems.

CRediT authorship contribution statement

S.K. Star: Conceptualization, Formal analysis, Investigation, Methodology, Software, Visualization, Writing – original draft. **L.F. Penuela Escobar:** Formal Analysis, Visualization, Writing – original draft. **M. van Meerkerk:** Conceptualization, Funding acquisition, Project administration, Writing – review & editing. **I.W.M. Pothof:** Writing – review & editing. **A.G.T.J. Heinsbroek:** Investigation, Resources, Writing – review & editing.

Funding sources

This work was supported by the Dutch Ministry of Economic Affairs and Climate via the SITO-IS subsidy, The Netherlands (grant number DGBI-I&K/41 032688).

Declaration of competing interest

The authors declare that they have no known competing financial interests or personal relationships that could have appeared to influence the work reported in this paper.

Acknowledgments

We want to thank colleague S van der Zwan for his consultation on Wanda.

Data availability

Data will be made available on request.

References

- [1] D.A.V. Duyne, M. Merilo, *Water Hammer Handbook for Nuclear Plant Engineers and Operators*, Electric Power Research Institute, 1996.
- [2] A. Bergant, A. Tijsseling, Y. Kim, U. Karadžić, L. Zhou, M.F. Lambert, A.R. Simpson, Unsteady pressures influenced by trapped air pockets in water-filled pipelines, *Strojniški vestnik-J. Mech. Eng.* 64 (9) (2018) 501–512, <http://dx.doi.org/10.5545/sv-jme.2018.5238>.
- [3] A. Kruisbrink, A. Heinsbroek, Fluid–structure interaction in non-rigid pipeline systems—large scale validation tests—(eureka project 274), in: *Pipeline Systems*, Springer, 1992, pp. 151–164, [http://dx.doi.org/10.1016/S0029-5493\(96\)01363-5](http://dx.doi.org/10.1016/S0029-5493(96)01363-5).
- [4] A. Bergant, A.R. Simpson, A.S. Tijsseling, Water hammer with column separation: A historical review, *J. Fluids Struct.* 22 (2) (2006) 135–171, <http://dx.doi.org/10.1016/j.jfluidstructs.2005.08.008>.
- [5] A. Bergant, J.M. van't Westende, T. Koppel, J. Gale, Q. Hou, Z. Pandula, A.S. Tijsseling, Water hammer and column separation due to accidental simultaneous closure of control valves in a large scale two-phase flow experimental test rig, in: *Pressure Vessels and Piping Conference*, Vol. 49224, 2010, pp. 923–932, <http://dx.doi.org/10.1115/PVP2010-26131>.
- [6] I. Pothof, B. Karney, Guidelines for transient analysis in water transmission and distribution systems, in: *Water Supply System Analysis-Selected Topics*, IntechOpen, 2012, pp. 1–21, <http://dx.doi.org/10.5772/53944>.
- [7] B. Skagestad, P. Mildenstein, *District Heating and Cooling Connection Handbook*, International Energy Agency IEA District Heating and Cooling, 2002.
- [8] S. Kuntuarova, T. Lickleder, T. Huynh, D. Zinsmeister, T. Hamacher, V. Perić, Design and simulation of district heating networks: A review of modeling approaches and tools, *Energy* (2024) 132189, <http://dx.doi.org/10.1016/j.energy.2024.132189>.
- [9] J. Hua, S. Zhang, L. Fu, Similitude criterion derivation and pipe physical property test and suitable analysis for water hammer scale model of long distance district heating pipeline, *Appl. Therm. Eng.* 125 (2017) 80–90, <http://dx.doi.org/10.1016/j.applthermaleng.2017.07.013>.
- [10] P.E. Grohnheit, B.O.G. Mortensen, Competition in the market for space heating. District heating as the infrastructure for competition among fuels and technologies, *Energy Policy* 31 (9) (2003) 817–826, [http://dx.doi.org/10.1016/S0301-4215\(02\)00666-6](http://dx.doi.org/10.1016/S0301-4215(02)00666-6).
- [11] Staatstoelicht op de Mijnen, Rapport Van Bevindingen Trias Westland Incident op 10 September 2021, Tech. Rep., 2022, Staatstoelicht op de Mijnen.
- [12] S. Werner, S. Andersson, E.-M. Abrahamsson, Fjärrvärmeolyckor : en Översiktlig Förstudie, Svensk Fjärrvärme, Stockholm, 2009.
- [13] S. Braungardt, V. Bürger, T. Fleiter, M. Bagheri, P. Manz, A. Billerbeck, K. Al-Dabbas, B. Breitschopf, J. Winkler, M. Fallahnejad, et al., Renewable heating and cooling pathways—towards full decarbonisation by 2050—final report, 2023.
- [14] Ministerie van EZK, Nationaal plan energiesysteem, 2023.
- [15] DNE Research, Nationaal Warmtenet Trendrapport 2021, Tech. Rep., 2021, on behalf of Stichting Warmtenetwerk.
- [16] T. Tereshchenko, N. Nord, Importance of increased knowledge on reliability of district heating pipes, *Procedia Eng.* 146 (2016) 415–423, <http://dx.doi.org/10.1016/j.proeng.2016.06.423>.
- [17] K. Rambøll, Cost Drivers in District Heating: Comparison of Capex Costs Between the Netherlands and Denmark, Tech. Rep., Danish Energy Agency and TNO, 2022.
- [18] D. Østergaard, S. Svendsen, Space heating with ultra-low-temperature district heating—a case study of four single-family houses from the 1980s, *Energy Procedia* 116 (2017) 226–235, <http://dx.doi.org/10.1016/j.egypro.2017.05.070>.
- [19] P. Verstraten, R. Niessink, F. Verheij, M. Duedahl, A. Huygen, *Best Practices for Planning and Construction of Thermal Networks Identified in the EU*, Tech. Rep., Publications Office of the European Union, 2021.
- [20] Euroheat & Power, Waste heat from data centre - Amsterdam, The Netherlands, 2024, URL <https://www.euroheat.org/dhc/knowledge-hub/1-17-datacentre-the-netherlands-amsterdam-in-operation>. (Accessed 27 August 2024).
- [21] Euroheat & Power, ReUseHeat project overview - data centre heat recovery in Berlin, 2024, URL <https://www.euroheat.org/dhc/knowledge-hub/re-use-heat-project-funded-by-horizon-2020>. (Accessed 27 August 2024).
- [22] Euroheat & Power, Hospital heat recovery - Madrid, Spain, 2024, URL <https://www.euroheat.org/dhc/knowledge-hub/1-4-hospital-heat-recovery-spain-madrid-in-operation>. (Accessed 27 August 2024).
- [23] F. Wernstedt, P. Davidsson, C. Johansson, Simulation of district heating systems for evaluation of real-time control strategies, in: *1st European Simulation and Modelling Conference*, Citeseer, 2003, pp. 1–7.
- [24] M.H. Elhafaia, A. Nova-Rincon, S. Sochard, S. Serra, J.-M. Reneaume, Optimization of the pipe diameters and the dynamic operation of a district heating network using a robust initialization strategy, *Appl. Therm. Eng.* 258 (2025) 124533, <http://dx.doi.org/10.1016/j.applthermaleng.2024.124533>.
- [25] T. Kallio, *Development and Validation of a Dynamic Simulation Model of a District Heating System (Master's thesis)*, Aalto University, 2020.
- [26] J. Zheng, Z. Zhou, J. Zhao, J. Wang, Function method for dynamic temperature simulation of district heating network, *Appl. Therm. Eng.* 123 (2017) 682–688, <http://dx.doi.org/10.1016/j.applthermaleng.2017.05.083>.
- [27] Y. Wang, X. Wang, L. Zheng, X. Gao, Z. Wang, S. You, H. Zhang, S. Wei, Thermo-hydraulic coupled analysis of long-distance district heating systems based on a fully-dynamic model, *Appl. Therm. Eng.* 222 (2023) 119912, <http://dx.doi.org/10.1016/j.applthermaleng.2022.119912>.
- [28] G. Hypolite, J.-H. Ferrasse, O. Boutin, S. Del Sole, J.-F. Cloarec, Dynamic modeling of water temperature and flow in large water system, *Appl. Therm. Eng.* 196 (2021) 117261, <http://dx.doi.org/10.1016/j.applthermaleng.2021.117261>.
- [29] I. del Hoyo Arce, S.H. López, S.L. Perez, M. Rämä, K. Klobut, J.A. Febres, Models for fast modelling of district heating and cooling networks, *Renew. Sustain. Energy Rev.* 82 (2018) 1863–1873, <http://dx.doi.org/10.1016/j.rser.2017.06.109>.
- [30] L. Giraud, R. Bavière, C. Paulus, M. Vallée, J.-F. Robin, Dynamic modelling, experimental validation and simulation of a virtual district heating network, in: *Proc. of the 28th Int. Conf. on Efficiency, Cost, Optimization, Simulation and Environmental Impact of Energy Systems, ECOS*, 2015, pp. 1–12.
- [31] E. Guelpa, Impact of network modelling in the analysis of district heating systems, *Energy* 213 (2020) 118393, <http://dx.doi.org/10.1016/j.energy.2020.118393>.
- [32] T. Oppelt, T. Urbanek, U. Gross, B. Platzer, Dynamic thermo-hydraulic model of district cooling networks, *Appl. Therm. Eng.* 102 (2016) 336–345, <http://dx.doi.org/10.1016/j.applthermaleng.2016.03.168>.
- [33] M. Paananen, T. Henttonen, Investigations of a long-distance 1000 mw heat transport system with APROS simulation software, in: *20th International Conference on Structural Mechanics in Reactor Technology, SMIRT 20*, 2009, pp. 1–10.
- [34] A. Kaliatka, E. Uspuras, M. Valincius, Analysis of dynamic processes during the accidents in a district heating system, *HEFAT 2012* (2012) 917–925, URL <http://hdl.handle.net/2263/43017>.
- [35] X. Zheng, B. Xu, Y. Wang, S. You, H. Zhang, S. Wei, N. Wang, Hydraulic transient modeling and analysis of the district heating network, *Sustain. Energy Grids Netw.* 25 (2021) 100409, <http://dx.doi.org/10.1016/j.segan.2020.100409>.
- [36] V.D. Stevanovic, B. Zivkovic, S. Prica, B. Maslovaric, V. Karamarkovic, V. Trkulja, Prediction of thermal transients in district heating systems, *Energy Convers. Manage.* 50 (9) (2009) 2167–2173, <http://dx.doi.org/10.1016/j.enconman.2009.04.034>.
- [37] J. Emadi, A. Solemani, Maximum water hammer sensitivity analysis, *World Acad. Sci. Eng. Technol.* 73 (2011) 416–419.
- [38] I. Bentley Systems, *WaterGEMS*, version 10.03.05.05, 2024, URL <https://www.bentley.com/en/products/product-line/hydraulics-and-hydrology-software/watergems>.
- [39] A. Dudlik, H.-M. Prasser, A. Apostolidis, A. Bergant, Water hammer induced by fast-acting valves: Experimental studies at pilot plant pipework, *Multiph. Sci. Technol.* 20 (3–4) <http://dx.doi.org/10.1615/MultScienTechn.v20.i3-4.20>.
- [40] A. Saidani, A. Fourar, F. Massouh, Numerical investigation of temperature effect on water hammer with cavitation in copper pipe rig, *J. Comput. Appl. Res. Mech. Eng. (JCARME)* 11 (2) (2022) 279–295, <http://dx.doi.org/10.22061/jcarme.2021.6961.1906>.
- [41] K. Urbanowicz, M. Firkowski, Parameters affecting water hammer in metal pipelines, in: *E3S Web of Conferences*, Vol. 44, EDP Sciences, 2018, pp. 1–8, <http://dx.doi.org/10.1051/e3sconf/20184400183>.
- [42] K. Urbanowicz, M. Firkowski, Parameters affecting water hammer in plastic pipelines, *Zeszyty Naukowe Akad. Morskiej Szczecinie* 54 (2018) 35–43.

- [43] G.S. Kell, Effects of isotopic composition, temperature, pressure, and dissolved gases on the density of liquid water, *J. Phys. Chem. Ref. Data* 6 (4) (1977) 1109–1131, <http://dx.doi.org/10.1063/1.555561>.
- [44] H. Gholizadeh, R. Burton, G. Schoenau, Fluid bulk modulus: A literature survey, *Int. J. Fluid Power* 12 (3) (2011) 5–15, <http://dx.doi.org/10.1080/14399776.2011.10781033>.
- [45] Y. Joliff, J. Absi, M. Huger, J. Glandus, Experimental and numerical study of the elastic modulus vs temperature of debonded model materials, *Comput. Mater. Sci.* 44 (2) (2008) 826–831, <http://dx.doi.org/10.1016/j.commatsci.2008.04.024>.
- [46] J.W.A.R. Manuel, C.B. Vreugdenhil, Waterslag, *Tech. Rep., Waterloopkundig Laboratorium Delft*, 1968.
- [47] The Engineering ToolBox, Metals and alloys - Young's modulus of elasticity, 2004, URL https://www.engineeringtoolbox.com/young-modulus-d_773.html. (Accessed 21 August 2024).
- [48] A. Drai, B. Aour, Analysis of the temperature effect on the behavior of high density polyethylene during high pressure torsion process, in: *21ème Congrès Français de Mécanique, CFM 2013*, 2013, pp. 1–6.
- [49] E. Guelpa, M. Capone, A. Sciacovelli, N. Vasset, R. Baviere, V. Verda, Reduction of supply temperature in existing district heating: A review of strategies and implementations, *Energy* 262 (2023) 125363, <http://dx.doi.org/10.1016/j.energy.2022.125363>.
- [50] H. Gadd, S. Werner, Achieving low return temperatures from district heating substations, *Appl. Energy* 136 (2014) 59–67, <http://dx.doi.org/10.1016/j.apenergy.2014.09.022>.
- [51] X. Wang, Uncertainty quantification and global sensitivity analysis for transient wave propagation in pressurized pipes, *Water Resour. Res.* 57 (4) (2021) 1–26, <http://dx.doi.org/10.1029/2020WR028975>.
- [52] A. Bergant, A.R. Simpson, A.S. Tijsseling, *Water Hammer with Column Separation: A Review of Research in the Twentieth Century, CASA-report 0434*.
- [53] O.M. Abdeldayem, D. Ferràs, S. van der Zwan, M. Kennedy, Analysis of unsteady friction models used in engineering software for water hammer analysis: Implementation case in wanda, *Water* 13 (4) (2021) 495, <http://dx.doi.org/10.3390/w13040495>.
- [54] Deltares, Wanda 4.7 User Manual, *Tech. Rep., Deltares*, 2023, URL <https://deltares-wanda-core.readthedocs-hosted.com/en/latest/#>.
- [55] M. Tukker, Wanda Validation Summary, *Tech. Rep., Deltares*, 2012, URL <https://publicwiki.deltares.nl/download/attachments/53542921/Wanda%20Validation%20report%202012.pdf>.
- [56] WL — Delft Hydraulics, Uncertainty Analysis (and more) in Wanda, *Tech. Rep., WL — Delft Hydraulics*, 2006, URL <https://publicwiki.deltares.nl/download/attachments/53542921/Wanda-uncertainty.pdf>.
- [57] S. Pal, P.R. Hanmaiahgari, B.W. Karney, An overview of the numerical approaches to water hammer modelling: The ongoing quest for practical and accurate numerical approaches, *Water* 13 (11) (2021) 1597, <http://dx.doi.org/10.3390/w13111597>.
- [58] A.K. Soares, N. Martins, D.I. Covas, Investigation of transient vaporous cavitation: experimental and numerical analyses, *Procedia Eng.* 119 (2015) 235–242, <http://dx.doi.org/10.1016/j.proeng.2015.08.881>.